universität wien

MASTERARBEIT / MASTER'S THESIS

Titel der Masterarbeit / Title of the Master's Thesis

„Characterization of a bipolar electrospray source for the stable generation of monomobile salt clusters in the size range of one to three nanometers“

verfasst von / submitted by

Julian Resch, BSc

angestrebter akademischer Grad / in partial fulfilment of the requirements for the degree of

Master of Science (MSc)

Wien, 2020 / Vienna 2020

Studienkennzahl lt. Studienblatt / degree programme code as it appears on the student record sheet:	A 066 876
Studienrichtung lt. Studienblatt / degree programme as it appears on the student record sheet:	Masterstudium Physik
Betreut von / Supervisor:	Assoz. Prof. Dr. Paul Winkler, Privatdoz.

Acknowledgements

First of all I want to thank Prof. Paul Winkler for giving me the opportunity to conduct my thesis in his group, I could not have asked for a better environment to do research and I am beyond grateful for this. His support and guidance where necessary throughout the whole time were inevitable factors for the completion of this thesis. Furthermore he enabled me to work as an academic researcher in Prof. Jim Smith's group alongisde Dr. Mike Lawler at UC Irvine and participate in the SeaScape campaign at Scripps Institute of Oceanography in San Diego on marine aerosol, where I expanded my field of knowledge in aerosol science and especially the chemical processes behind it tremendously, which I am extremely thankful for.

Next I want to thank Dr. Gerhard Steiner for his role as a mentor throughout my bachelors and master thesis and for introducing me to the aerosol group. If it wasn't for him I would have never been able to join Prof. Winklers group nor experience the great world of aerosol science.

Furthermore I want to thank the group members Paulus Bauer, Sophia Brilke, Loic Gonzalez Carracedo, David Schmoll, Manuel Schöberl, Christian Tauber, Miguel Vazquez Pufleau, Daniela Wimmer and Peter Wlasits, and Markus Leiminger, whom I enjoyed working with and who supported me throughout my time in the lab and countless visits to the coffee machine. I am especially grateful for the mentoring of Sophia Brilke, I truly could not have asked for someone better, not only did she have the patience to teach me everything necessary to complete this thesis but moreover she was always there to answer my questions or help. I will never forget the countless hours spent in both the office and lab, talking about the experiments or possible next steps and our friday evening braingasms and outbursts of laughter. The question "What would Gerhard say?" on a Friday evening never meant we immediately left the lab but I never regreted spending longer days at University in such great company.

By far my deepest appreciation, not only regarding my studies, but life in general go out to my parents, Stephanie and Armin Resch. Not only have they supported and encouraged me throughout every decision I made in life but they have always enabled me to achieve my goals and dreams.

Additionally I want to thank my former class teacher Mag. Helga Kudler for her great enthusiasm put into teaching math and physics which let me discover my interest in physics at a young age and planting the seed in my head to study physics. Lastly I want to thank all my friends for their support.

Abstract

Generating mobility standards has been of great importance for characterization and calibration of instruments in aerosol research. A common method of generating sub-2nm standards is the use of unipolar electrospray sources, which has been limited to the first few clusters. In this study a bipolar electrospray source is introduced to significantly extend the range of available singly charged clusters through charge reduction. The use of a high resolution differential mobility analyzer (UDMA) in combination with an Atmospheric Pressure interface Time-of-Flight Mass Spectrometer (ioniAPi-ToF MS, Ionicon Analytik GmbH, Austria) enabled detailed characterization of the electrical mobility and chemical composition (mass-to-charge ratio) of different tetra-alkyl ammonium halide clusters, generated by the bipolar electrospray source. Different operating settings were tested and characterized. The unipolar and bipolar mobility spectra for both positive and negative salt clusters are presented. The individual peaks are analyzed to confirm the successful charge reduction by the bipolar electrospray source and to reassure that dominantly singly charged salt clusters are produced which is required for subsequent instrument characterization. The obtained mobility standards were used to characterize an ultrafine condensation particle counter (TSI Model 3776 UCPC). Furthermore, a detailed operating manual for the bipolar electrospray source was established.

Zusammenfassung

Die Erzeugung von Mobilitätsstandards ist ein wichtiger Bestandteil der Aerosolforschung. Eine weit verbreitete Methode um sub-2nm Standards zu generieren sind Elektrosprays. In dieser Studie wird eine Bipolare Elektrospray Quelle präsentiert, um den Bereich der verfügbaren einfach geladenen Salzcluster durch Ladungsreduktion zu erweitern.
Die Verwendung eines hoch auflösenden Differentiellen Mobilitäts Analysators in Kombination mit einem Massenspektrometer ermöglichten detaillierte Charakterisierung der elektrischen Moblität und Masse von verschiedenen in Acetonitril gelösten Tetra-Alkyl Ammonium Haliden. Verschiedene Einstellungen wurden getestet und charakterisiert. Die Mobilitätsspektren für positive und negative Salz Cluster wurden präsentiert. Die individuellen Peaks wurden analysiert um zu bestätigen, dass mit der Bipolaren Elektrospray Quelle die Ladung der Cluster erfolgreich reduziert werden kann und dass es sich dabei um einfach geladene Salz Cluster handelt. Die erhaltenen Mobilitätsstandards wurden verwendet, um einen Kondensationskernzähler zu charakterisieren. Weiters wurde eine detaillierte Bedienungsanleitung für die Bipolare Elektrospray Quelle erstellt.

Contents

1 Introduction

Aerosols play an important role in our everyday lives. Not only are we constantly surrounded by aerosols, but they are also now more than ever present in the media. Shall it be the laws regarding smoking in Austria, which ultimately effects our health [Cheng et al., 1990], or pollution related topics all over the world. Especially when one sees media coverage of images of air quality in bigger cities in Asia their significant contributions are highlighted [Mönkkönen et al., 2004, Colbeck and Lazaridis, 2010]. To list a couple of other effects that can be related to aerosols one can consider the optical effects caused by their presence in the atmosphere. As well as new particle formation (NPF) and its contribution to cloud condensation nuclei (CCN) formation, which has direct impact on the atmosphere and the Earths climate system [Spracklen et al., 2008, Bzdek and Johnston, 2010, IPCC, 2013, Gordon et al., 2017]. Along with their use in drug delivery to the lung through nose- or mouthsprays [Hinds, 1999].
When speaking of aerosols one refers to a two-phase system consisting of solid or liquid particles suspended in a carrier gas where their size ranges from single digit nanometers to more than 100 µm. Different sized Aerosol particles can ultimately be traced back to their different origins.
Aerosols can be grouped into primary and secondary aerosol. The former refer to particles directly introduced into the atmosphere while the latter relate to aerosol particles which are formed by chemical reactions of gaseous components (gas-to-particle conversion). Both can have either anthropogenic or natural origin. Anthropogenic aerosol directly emitted include direct emissions from industry or fossil fuel combustion. Directly emitted aerosol of natural sources include sea spray, dust being blown into the atmosphere by wind, forest fires or volcano eruptions. Secondary aerosol is mainly formed by homogeneous nucleation, including processes such as new particle formation through different vapors. These low-volatile vapors can have anthropogenic or natural origin, including things such as anthropogenic emissions or gas generation through forests or over the ocean [Hinds, 1999]. To better understand atmospheric climate effects and new particle formation it is inevitable to have detailed knowledge of the aerosol number concentration of single digit nm particles, which is an important measured property of aerosols and is usually given in number of particles per volume [Hinds, 1999, Kulmala et al., 2013]. The ability to measure nanometer sized particles immensely improved through the introduction of Differential Mobility Analyzers (DMA), and different types of particle counters such as Faraday Cup Electrometers (FCE), Condensation Particle Counters (CPC) and others [Flagan, 1998]. Several different methods are used for generating sub-5nm test aerosol particles to calibrate particle counters [Kangasluoma et al., 2013, Wimmer et al., 2013, Kangasluoma et al., 2014], one of them being an electrospray source for the generation of sub-2nm particles [Ude and Fernández de la Mora, 2005, Fernandez de la Mora et al., 2005, Jiang et al., 2011]. This method has been limited to the first few clusters $(A^{+/-})_{n+1}(AB)_n$ (n=0,1) of salts, $(A^{+/-})$ representing the cations and (AB) the neutral pairs in the cluster. As the higher complex clusters seem to carry multiple charges and therefore can not be unambiguously resolved by mobility anymore, resulting

in the distinct separation of salt clusters (e.g. tetra-heptyl ammonium bromide (THABr)), typically being limited to mobility equivalent diameters in the range around ≈1.7nm [Fernandez de la Mora and Barrios-Collado, 2017].
The introduction of a bipolar electrospray source, which combines two oppositely charged electrospray tips in one electrospray chamber, as described by Fernandez de la Mora and Barrios-Collado (2017), extends the size range of singly charged clusters to higher values of n. The aim of this thesis is to characterize the bipolar electrospray source in combination with a Vienna-type high resolution DMA (UDMA) [Steiner et al., 2010] and an Atmospheric Pressure interface Time-of-Flight Mass Spectrometer (ioniAPi-ToF MS, Ionicon Analytik GmbH, Austria). Experiments were conducted to investigate different operating settings of the bipolar electrospray, to obtain mass and mobility spectra of the generated molecular clusters, to confirm the charge state of the produced clusters and to perform counting efficiency measurements using an ultrafine condensation particle counter (UCPC).

2 Background Information and Experimental Methods

2.1 Aerosol Generation

The generation of test aerosols is one major topic of aerosol technology as they are necessary for conducting aerosol research and instrument calibration. To investigate the effect of particle size on sampling devices and the calibration of particle-size measuring instruments, a stable source of test aerosol is obligatory. This test aerosol is usually polydisperse and can either be charged or uncharged. An ideal aerosol generator is best characterized by a constant and reproducible output of stable aerosol [Hinds, 1999]. In order to obtain monodisperse aerosol where particles have little deviation in regard to shape and size out of a test aerosol, classification is necessary and will be discussed in section 2.2 Aerosol Classification. In this study, bipolar test aerosol was generated by the bipolar electrospray source run in either unipolar or bipolar mode.

2.1.1 Electrospray Ionization

The introduction of electrospray ionization (ESI) by Fenn et al. [Fenn et al., 1989] made molecular clusters in the small nm size range accessible for different fields of studies. In the case of aerosol science it has been widely used for generation of mobility and mass standards [Ude and Fernández de la Mora, 2005, Fernandez de la Mora et al., 2005]. Generally, an analyte sample is transferred from the liquid phase to the gas phase. The analyte sample is dissolved in a polar liquid, such as acetonitrile, methanol or water and then raised to a high voltage potential. This liquid is then pushed through a capillary by applying a pressure in the range of 5-100 mBar and subsequently exposed to a strong electric field inside of an electrospray chamber. Upon exposure to the electric field a surface charge is induced on the liquid, forcing it into a so called "Taylor Cone" (due to the balance between surface tension and electrical forces) [Taylor, 1964]. At the tip of the Taylor Cone a jet of highly charged unipolar droplets enters the chamber. The droplets become smaller as the liquid solvent evaporates. Upon reaching and exceeding Rayleigh's charge limit, coulombic fission of the droplets results in small charged particles or clusters exiting the electrospray chamber (see Figure 1) [Steiner, 2011, Kangasluoma, 2015].

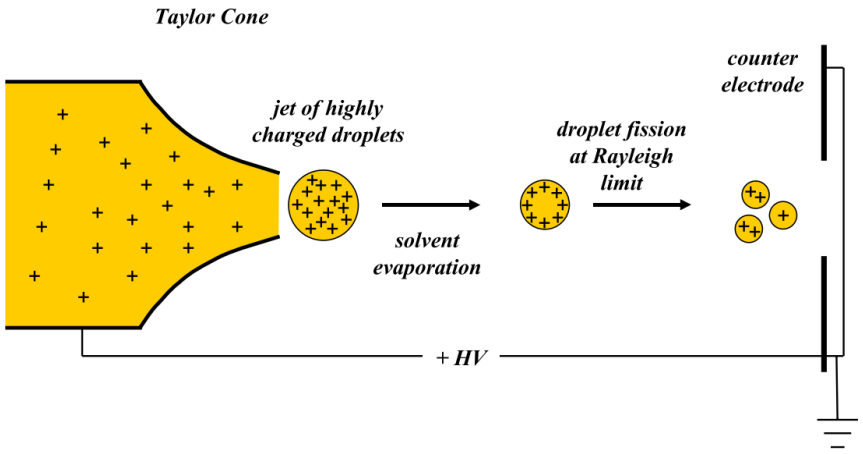

Figure 1: Illustration of the working principle of an electrospray being run in positive ion mode, image taken from [Steiner, 2011].

2.1.2 Bipolar Electrospray

The bipolar electrospray source (ES) as introduced by Fernandez de la Mora and Barrios-Collado (2017) and the following work [Fernandez de la Mora, 2018] is commercially available by SEADM, S.L., Spain. The bipolar ES combines two electrospray capillaries set to opposite polarities inside of a stainless-steel chamber with two windows on the top and bottom and an aerosol inlet and outlet along one axis with a 50 % transparent stainless-steel mesh separating the two capillary tips electrostatically. At a 45° angle with respect to this axis the two capillary tips are positioned in the chamber (see Figure 2 and 3), the other ends of the capillaries are inserted into two separate vials (see Figure 4) where they are alongside an electrode inside of a solution.

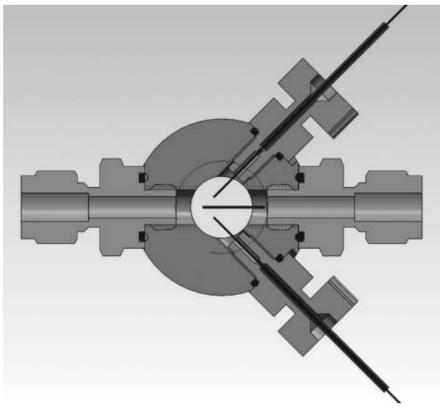

Figure 2: Illustration of the bipolar ES source chamber from an aerial view. The gas flow is introduced to the chamber from the right inlet where the stainless-steel "half mesh" is mounted and is separating the two capillary tips spraying in opposite polarities, which are placed at a 90° angle with respect to each other. On the left side the aerosol exits the chamber. Image taken from [Fernandez de la Mora, 2018].

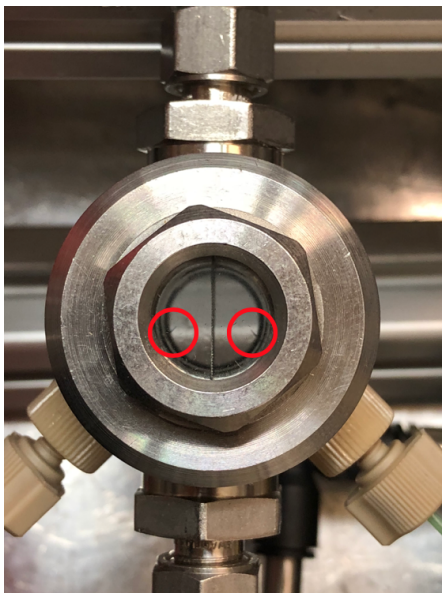

Figure 3: The bipolar electrospray chamber. The capillary tips are circled in red. The "full mesh" is separating the chamber halfs. Image was taken at the Faculty of Physics, University of Vienna.

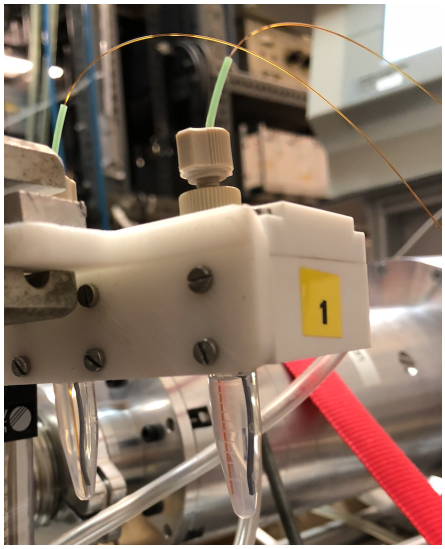

Figure 4: The vials of the bipolar electrospray source containing the capillaries (copper), electrodes (grey) and solutions for both polarities. Image was taken at the Faculty of Physics, University of Vienna.

Lowering the background in mobility spectra, generated through multiply charged clusters at higher mobilities, is a goal of charge reduction methods [Attoui et al., 2013]. One method is the neutralization through exposure to ions of opposite polarity by an aerosol neutralizer, with the shortcoming that the exact chemical composition of the produced clusters is not known [Steiner et al., 2017]. The essential advantage of the bipolar electrospray in charge reduction is the combination of oppositely charged electrosprays with solutions containing the same salts [Fernandez de la Mora and Barrios-Collado, 2017]. Therefore knowing the exact

composition of the sprayed ions and their counter-ions leads to knowledge of the composition of the anion and cation. The challenge when trying to electrospray two different polarities in the same chamber is to electrostatically isolate the two regions from each other. As recently demonstrated the technique of separating the chamber halfs with a grounded mesh is a viable solution to this problem, allowing the tips to be close to each other while still not interfering with their counterpart. Thus leading to a one parameter n dependency in the cluster composition of the sprayed salt-solutions and therefore extending the range of singly charged clusters to higher orders [Fernandez de la Mora and Barrios-Collado, 2017].

2.1.3 Solutions used for Electrospraying

Previous studies have shown that solutions of tetra-alkyl ammonium halides are well suited for cluster generation by means of electrospray ionization [Ude and Fernández de la Mora, 2005, Fernandez de la Mora et al., 2005, Steiner et al., 2010, Kangasluoma et al., 2013]. Therefore in this study three different salts have been dissolved in acetonitrile (HPLC grade acetonitrile, CAS: 75 - 05 - 8, Sigma - Aldrich) at concentrations of 1 mMol/L for the characterization of the bipolar electrospray source. The salts used are tetra-heptyl ammonium bromide (THABr, CAS: 4368-51-8, Sigma - Aldrich), tetra-butyl ammonium iodide (TBAI, CAS: 311-28-4, Sigma - Aldrich) as well as tetra-methyl ammonium iodide (TMAI, CAS: 75-58-1, Sigma - Aldrich). The produced clusters of the form $(A^{+/-})_{n+1}(AB)_n$, with n=0,1,2,..., and their inverse mobility (1/Z [Vs/cm^2]), the mobility equivalent diameter (d_p [nm], according to Equation 4) and mass over charge of the first isotope (m/z [Th] or assuming z=1 [amu]) of the singly charged clusters for each salt are given in Table 1.

	THABr	A^+		THABr	A^-		TBAI	A^+		TBAI	A^-		TMAI	A^+	
	1/Z	dp	m/z	1/Z	dp	m/z	1/Z	dp	m/z	1/Z	dp	m/z	1/Z	dp	m/z
$(AB)_0$	1.03	1.45	410.47	0.44	0.95	78.91	0.71	1.21	242.28	0.48	0.99	126.90	0.46	1.05	74.15
$(AB)_1$	1.52	1.77	899.86	0.95	1.40	568.30	1.09	1.50	611.47	0.85	1.32	496.09	0.68	1.20	275.20
$(AB)_2$	1.89	1.97	1389.25	1.30	1.63	1057.70	1.39	1.69	980.66	1.22	1.58	865.28	0.92	1.39	476.25
$(AB)_3$	2.23	2.14	1878.64	1.62	1.82	1547.09	1.57	1.79	1349.85	1.42	1.71	1234.47	-	-	677.30
$(AB)_4$	2.45	2.25	2368.03	1.92	1.99	2036.48	1.81	1.93	1719.04	1.70	1.87	1603.66	-	-	878.35
$(AB)_5$	2.79	2.40	2857.42	2.19	2.12	2525.87	2.09	2.07	2089.23	1.98	2.02	1972.85	-	-	1079.40
$(AB)_6$	3.13	2.54	3346.81	2.45	2.25	3015.26	-	-	2458.42	-	-	-	-	-	1280.45
$(AB)_7$	-	-	-	2.71	2.36	3504.65	-	-	2827.61	-	-	-	-	-	1481.50
$(AB)_8$	-	-	-	2.97	2.47	3994.04	-	-	3196.80	-	-	-	-	-	1682.55

Table 1: Table displaying the inverse mobilities (1/Z [Vs/cm^2]), mobility equivalent diameter (d_p [nm]) and atomic mass (m/z [Th]) of the salts used in the frame of this work. Values according to the measurements done in this thesis and [Ude and Fernández de la Mora, 2005, Steiner, 2011, Fernandez de la Mora and Barrios-Collado, 2017, Brilke et al., 2020]

2.2 Aerosol Classification

Particle size for small particles in aerosol science mostly refers to the electrical mobility equivalent diameter d_p, which is linked to the electrical mobility, Z, of a charged particle, essentially describing a charged particles path through an electric field in a certain medium. This relation will be discussed in further detail in the following chapter. To be able to analyze the number size distribution of atmospheric aerosol or to classify a specific monomobile/monodisperse aerosol out of a broad spectrum of polymobile/polydisperse aerosol, a so called Differential Mobility Analyzer (DMA) is used [Ude, 2004, Steiner, 2011]. Main contributions to the development of DMAs were made by several different authors [Knutson and Whitby, 1975, Reischl, 1991, Winklmayr et al., 1991], while a general overview of the history of electrical aerosol measurements is given in Flagan (1998).

2.2.1 Differential Mobility Analyzer

There are different DMA designs such as radial, planar or cylindrical DMAs. As the general working principle remains the same among the different types, only the cylindrical so called Vienna-type DMA will be explained in this chapter, following the overview given by [Knutson and Whitby, 1975, Reischl, 1991, Flagan, 1998, Steiner et al., 2010, Steiner, 2011].
The Vienna-type DMA is a cylindrical capacitor. A schematic cross section of a Vienna-type DMA is presented in Figure 5. The crucial parameters describing a DMAs overall performance can be separated into two categories, the geometry parameters which are fixed and the operating conditions which can be varied. A DMA can be described by the outer radius of the inner electrode R_1, the inner radius of the outer electrode R_2 and the length L which gives the distance between the aerosol inlet slit and the aerosol sampling or outlet slit. The operating conditions on the other hand are given by the sheath air flow rate Q_{sh}, the exhaust air flow rate Q_{ex}, the aerosol flow rate Q_a and the aerosol sample flow rate Q_s. In the case of the Vienna-type the purified sheath air is introduced tangentially into the DMA where it is then laminarized by a nylon mesh. This laminarization process of the sheath air is a crucial aspect of creating conditions where measurements with a DMA can be conducted. If there is turbulent sheath air flow inside of the DMA it will lead to non-idealities in the resulting mobility spectrum. In general the aim is to assure that ideally both pairs, Q_{ex} and Q_{sh} as well as Q_a and Q_s, are symmetrical, so that optimal operating conditions are given. Additionally the aerosol inlet flow is tangentially led into an annular cavity contained in the outer electrode. Through a symmetric pressure drop at the inlet slit the aerosol flow is smoothly transitioned into the sheath air. To select particles according to their electrical mobility an electric field inside of the DMA is necessary. Therefore a high voltage potential in either polarity can be applied to the inner electrode. Upon merging with the surrounding sheath air which forces the aerosol particles to move downstream, the electric field will attract certain ones towards the inner electrode. The particles with the corresponding electrical mobility will drift towards a small exit slit on the inner electrode.
Equation (1) shows the relation between the electrical mobility and the voltage applied to

the inner electrode [Steiner, 2011]:

$$Z = \frac{1}{V} \cdot \frac{\ln(\frac{R_2}{R_1})}{2 \cdot \pi \cdot L} \cdot \frac{(Q_{sh} + Q_{ex})}{2}. \tag{1}$$

Additionally, Z can be expressed in terms of the mobility equivalent particle diameter d_p,

$$Z = \frac{i \cdot e_0}{3 \cdot \pi \cdot \eta} \cdot \frac{C(d_p)}{d_p}, \tag{2}$$

where i is the number of elementary charges a particle is carrying, e_0 is the elementary charge, η the dynamic viscosity of the gas (for air: $\eta_{air} = 1.825 \cdot 10^{-5}$ [Pa · s] at 20°C and 1 atm) and $C(d_p)$ is the Cunningham slip correction factor [Cunningham, 1910]. Throughout this thesis the Cunningham slip correction factor was defined according to Equation (3) with the constants chosen as described in Reischl (1991), [Reischl, 1991],

$$C(d_p) = 1 + 2.492 \cdot (\frac{\lambda}{d_p}) + 0.840 \cdot (\frac{\lambda}{d_p}) \cdot \exp(-0.430 \cdot (\frac{\lambda}{d_p})), \tag{3}$$

where λ describes the mean free path of the surrounding gas molecules, which for air is $\lambda_{air} = 65.3$nm at 1 atm and 20°C [Reischl, 1991, Hinds, 1999].
The calculations done in the frame of this thesis for the (approximate) mobility equivalent diameter were conducted using an empirical approximation [Mäkelä et al., 1996], which is valid for the size range of 0.5nm $< d_p <$ 5nm, as seen in Equation (4),

$$Z = 2.2458 \cdot 10^{-22} \cdot d_p^{-1.9956}, \tag{4}$$

where (under the assumption of singly charged particles) Z is given in [m^2/Vs] and the diameter respectively in [m].

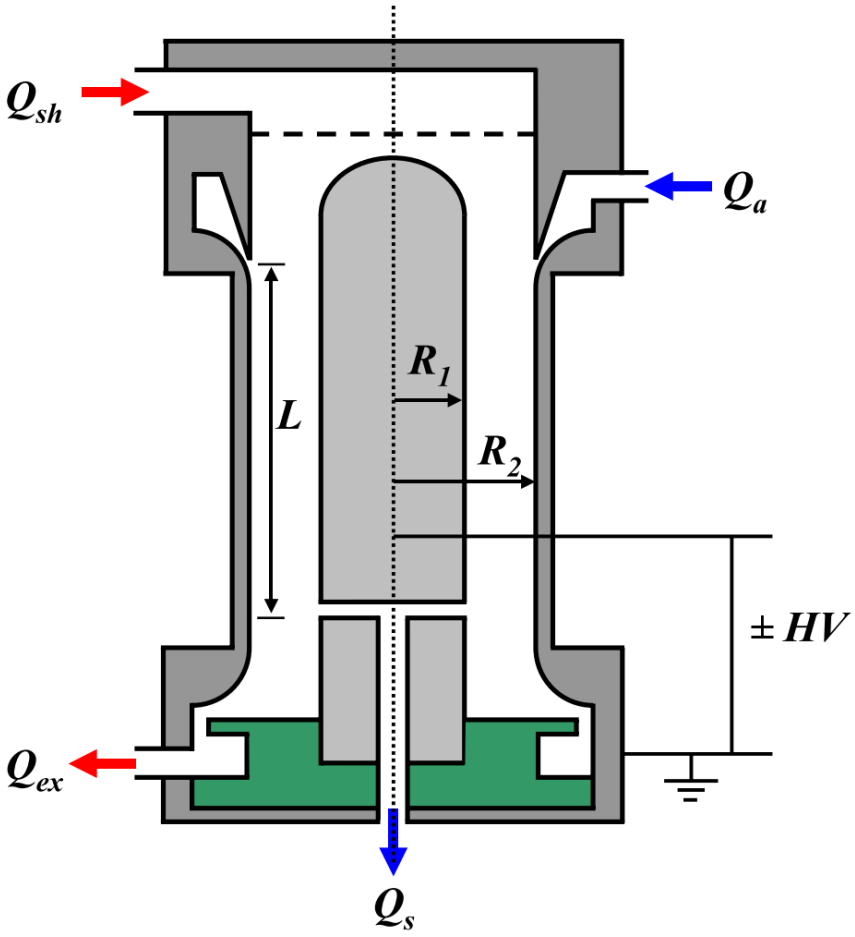

Figure 5: Schematic cross section of a Vienna-type DMA with the radius of the inner R_1 and outer electrode R_2, the distance L between aerosol inlet and outlet slit, the sheath air flow rate Q_{sh}, exhaust air flow rate Q_{ex}, aerosol inlet flow rate Q_a and aerosol sample flow rate Q_s. Image taken from [Steiner et al., 2010]

2.2.2 Vienna-type high resolution DMA

The latest version of the original UDMA1 ([Steiner et al., 2010, Steiner, 2011]), the so called UDMA4 (an image of both the UDMA1 and the UDMA4 and their corresponding instrument racks can be seen in Figure 6), was used for the experiments performed in this thesis. The UDMA4 has also been used in Brilke et al. (2020) where results have been published. The sheath air in the UDMA4 is introduced inline and not tangentially, causing less turbulence in the system. Through improved blowers and sheath air systems, higher flow rates are feasible. Otherwise the principle and geometrical properties of both UDMAs remained the same.

High-resolution mobility measurements in the size range of 1-5 nm for the investigation of small clusters is what the UDMA was built for. This is realized by achieving aerosol sheath air flow rates of up to 1000 L/min. The sheath air runs in a closed loop system with different gas cleaning filters to maintain the purity of the sheath air and therefore not affect further measurements by impurities in the system. A schematic of the UDMA4 can

be seen in Figure 7. The geometrical parameters of the UDMA4 are as follows: L=6.5mm, R_1=17.5mm, R_2=24mm. The DMA's resolution power can be defined, under the assumption of symmetrical flow conditions, as:

$$R = \frac{Q_a}{Q_{sh}}, \tag{5}$$

Alternatively to this definition, the resolution of a specific DMA can be determined with the ratio of the full width at half maximum, ΔZ, of a peak and the position of the peak maximum, Z^*. In this explanation the mobility spectrum abscissa is chosen as the electrical mobility Z, analogously this can be calculated for V or d_p as well.

$$R = \frac{\Delta Z}{Z*}. \tag{6}$$

The resolution power R_F, which is defined as the inverse of the previous R, can be written as [Flagan, 1999]:

$$R_F = \frac{Z^*}{\Delta Z}. \tag{7}$$

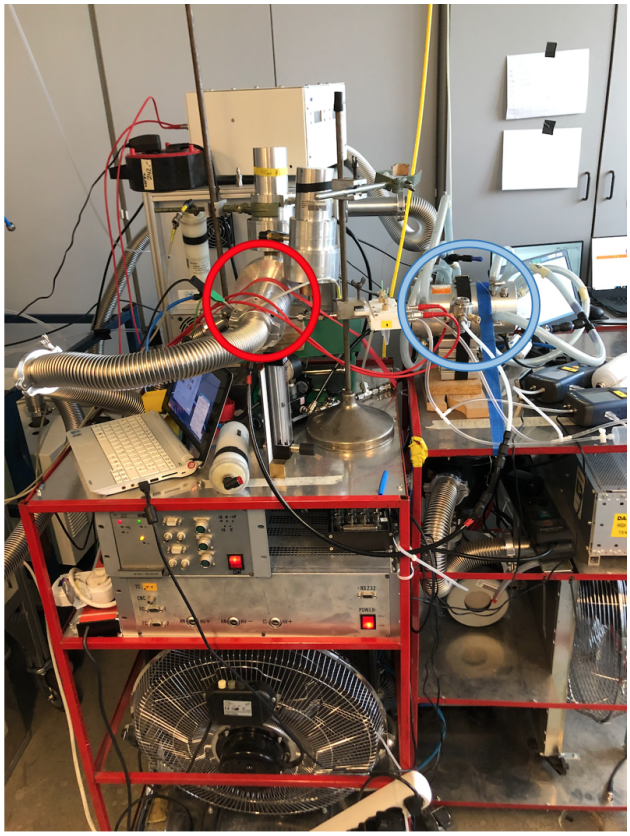

Figure 6: Tandem UDMA setup consisting of the original UDMA1 [Steiner et al., 2010, Steiner, 2011] on the right side (circled blue) and its blower rack along with the HV supplies and the UDMA4 (circled in red) on the left side with its corresponding rack.

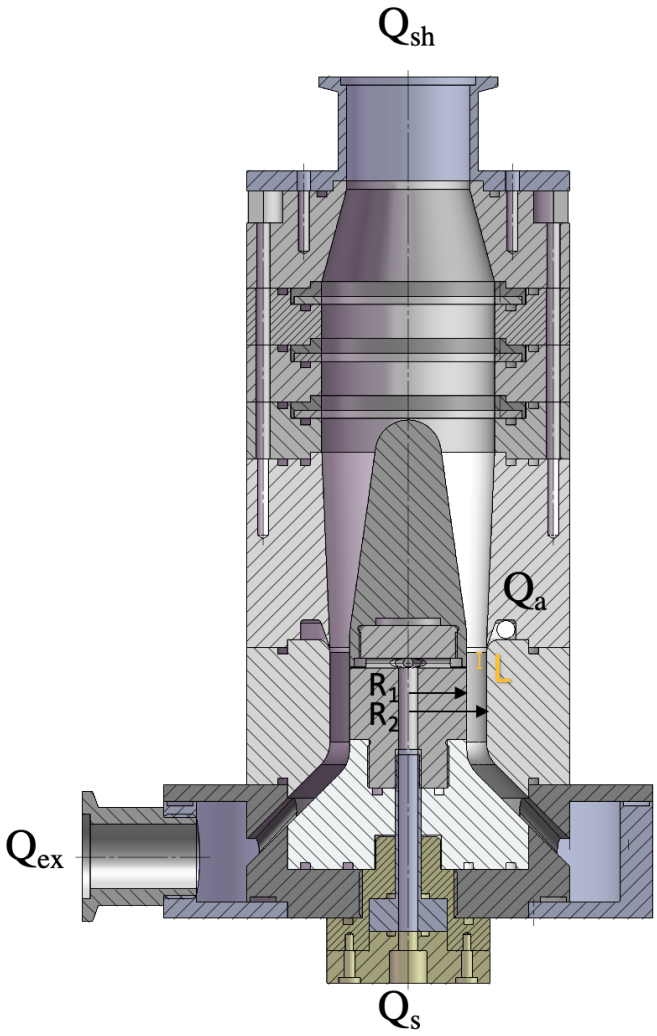

Figure 7: Schematic of the UDMA4, where the sheath air enters inline and not as in previous models tangentially. The geometrical parameters being: L=6.5mm, R_1=17.5mm, R_2=24mm. Image taken from Steiner with his permission [Steiner et al., 2018].

2.2.3 Calibration of the UDMA

Unlike DMAs running on lower sheath flows, the UDMA4 runs at flow rates up to 1000 L/min. Since it is hard to measure air flows at such high rates, the DMAs need another form of calibration that assigns electrical mobility to set DMA voltage. In order to calibrate the UDMA4 on a daily basis, which is necessary due to deviations in the exact sheath air flow rate, an aerosol of known properties is fed into the system. The corresponding mobility spectrum is recorded and through Equation (8) the correlation of the electrical mobility and the voltage set at the DMA for a given peak is obtained [Steiner et al., 2010].

$$Z = V^{-1} \cdot K, \tag{8}$$

where K describes the geometrical and operating parameters

$$K = \frac{\ln(\frac{R_2}{R_1})}{2 \cdot \pi \cdot L} \cdot Q_{sh}. \tag{9}$$

With this method the UDMA is calibrated and subsequent calculations of d_p can be performed knowing Q_{sh}.

2.3 Aerosol Detection

In the frame of this thesis three different types of detection devices were used, a TSI Model 3776 UCPC (TSI inc., Minneapolis, USA), an ioniAPi-ToF mass spectrometer used to measure the chemical composition of the aerosol particles and a fast response FCE [Winklmayr et al., 1991] which was used to record mobility spectra and as a reference counter for the calibration of the UCPC.

2.3.1 Condensation Particle Counter

Condensation Particle Counters (CPC) or Condensation Nuclei Counters are devices used for real-time measurements of particles and the particle number concentration [Stolzenburg and McMurry, 1991, Hinds, 1999], sometimes earning them the description as the backbone of aerosol research [Kangasluoma, 2015]. A brief history of these instruments was given by McMurry [McMurry, 2000]. CPCs detect nanometer size particles by optical detection after condensational growth. Different working fluids such as water, butanol or diethylen glycol (DEG) are used to create vapor inside of a CPC, in the frame of this thesis only butanol-based CPCs and their working principles will be discussed. Aerosol enters a CPCs saturator where it is exposed to saturated vapor which further leads to vapor condensation on particles which act as droplet seeds. These droplets grow to sizes where they can be detected by a laser, lenses and a photodiode inside of the optical block which is a substantial part of CPCs. Essentially, CPCs consist of three main parts, a saturator, a condenser and the previously mentioned optics block. Their working principle can be broken down into two steps, vapor nucleation on the particles followed by condensational growth into droplets large enough to be optically detected. The saturator usually consists of a wick connected to a reservoir of a given working fluid, at a higher temperature T_h, compared to the lower temperature in the condenser T_c. Inside the saturator the aerosol is exposed to saturated vapor of butanol. The aerosol then enters the colder condenser region, where supersaturation of the vapor leads to condensation onto the particles causing heterogeneous nucleation and droplet growth. In the last step, after the aerosol is focused by a nozzle, these droplets are measured. Each droplet accounting for a single droplet seed particle. A schematic of the working principle of a basic CPC is given in Figure 8 showing the different regions as mentioned above.

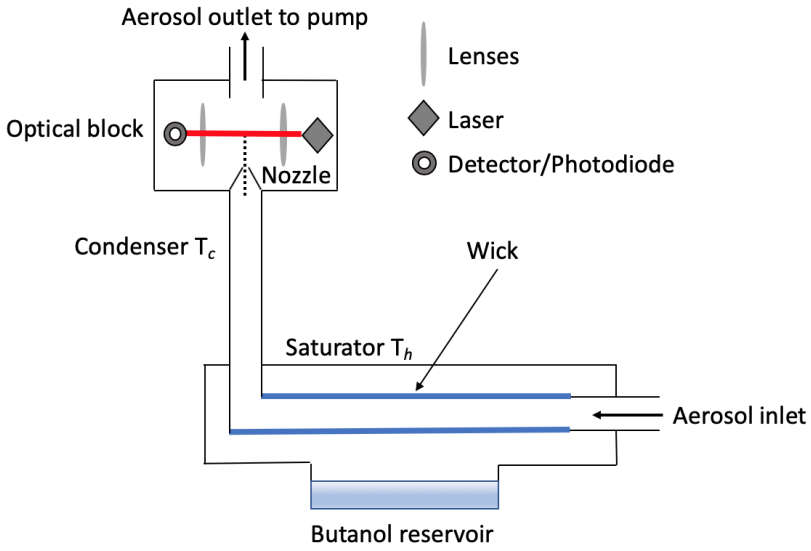

Figure 8: Schematic of the basic working principle of a CPC, containing the saturator with wick and butanol reservoir, the condenser and the optical block. $T_h > T_c$. Based on McMurry (2000).

2.3.2 Cut-off Diameter

The counting efficiency, ϵ, of a CPC is directly connected to the instrument's cut-off diameter, d_{50}, both of which are important for the characterization of CPCs for further evaluation of aerosol measurements [Stolzenburg and McMurry, 1991, Wimmer et al., 2013]. The cut-off diameter usually describes the lower detection limit of a CPC and is defined as the diameter where 50% of particles are still detected. Using UCPCs with low cut-offs is crucial for measuring ultrafine aerosol ($d_p \leq 20$nm) precisely and therefore better understanding the process of NPF in the atmosphere [Stolzenburg and McMurry, 1991]. The counting efficiency is calculated under use of Equation (10):

$$\epsilon = \frac{N_{CPC}}{N_{FCE}} \tag{10}$$

where N_{CPC} describes the number concentration of the CPC and N_{FCE} is the number concentration of the reference device, in this study a FCE respectively. An FCE, explained in section 2.3.5 Faraday Cup Electrometer, was selected to further verify that the classified singly charged clusters are indeed singly charged if ϵ reaches values of 1, as the FCE only accounts for charges independent of particle size.

Each CPC also has a detection efficiency, η_{total}, itself, accounting for the efficiency at which particles are detected $\eta_{detection}$, the activation efficiency $\eta_{activation}$ and the sampling efficiency $\eta_{sampling}$ which accounts for the ratio of the number concentration of particles entering and leaving the device, given in Equation (11) [Stolzenburg and McMurry, 1991]:

$$\eta_{total} = \eta_{activation} \cdot \eta_{sampling} \cdot \eta_{detection} \tag{11}$$

Each of these parameters are size dependent. The extension of the available size range of singly charged clusters by electrospraying aims to cover the necessary sizes to obtain a counting efficiency curve for a UCPC and measure its cut-off diameter.

2.3.3 TSI Model 3776 UCPC

The TSI Model 3776 UCPC (TSI inc., Minneapolis, USA), in the following often referred to as "3776", is a commercially available n-butanol-type UCPC built on the principles of the design of Stolzenburg and McMurry (1991). The flow path inside of the 3776 and it's working principle is discussed in this following section and can be seen in Figure 9. Additionally for these measurements the 3776 was operated under "tuned" conditions, meaning the temperature settings inside of the CPC were modified from custom settings to increase the supersaturation and therefore enhance the detection efficiency [Barmpounis et al., 2018]. The modified temperature settings will be given in section 4.2 Experimental Setups.

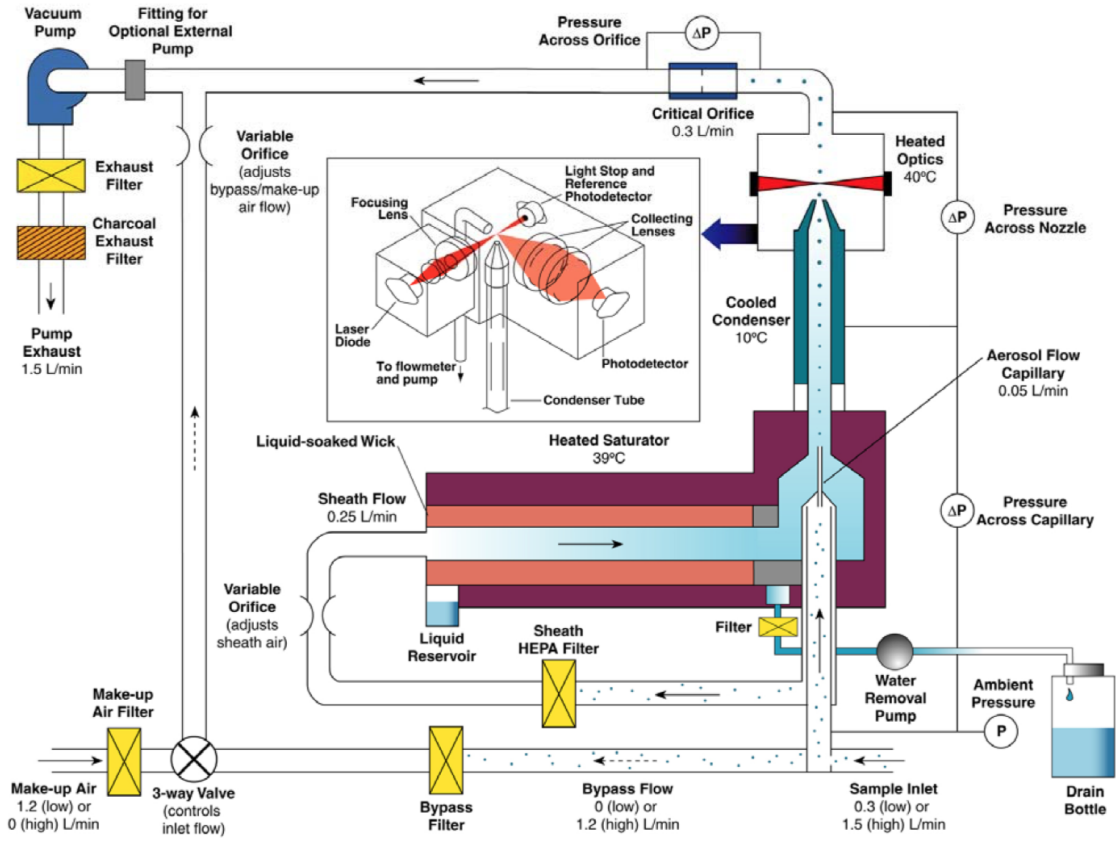

Figure 9: Schematic of the Flow inside the TSI Model 3776 UCPC, image taken from the TSI operation and service manual [TSI, 2019].

The main difference of the 3776 to the previously explained basic CPC working principle/layout (see Figure 8) is the splitting of the sample flow. In high flow mode the inlet flow (1.5 L/min) is split into a bypass flow (1.2 L/min) and a sensor flow (0.3 L/min). This sensor flow is split again into a capillary flow (0.05 L/min) and a sheath flow (0.25 L/min),

explaining why it is often referred to as a capillary-sheath structure [Takegawa et al., 2017]. This has the advantage of securing that the aerosol particles are confined to the centerline of the condenser and therefore passing the region with the highest supersaturation of n-butanol vapor [Tauber et al., 2019b]. Additionally any unnecessary condensed water or butanol is removed from the system. Several different pressure sensors across the UCPC constantly track the pressures inside allowing to maintain optimal working conditions even when raising the sample inlet flow to 2.5 L/min with an external pump. Increasing the sample flow rate leads to decreasing particle losses through diffusion. The sensor flow has to remain constant, while the valve controlling the make-up flow is adjusted so the inlet flow is raised to 2.5 L/min (this is performed by attaching a flowmeter to the inlet). The sheath-air valve is readjusted as well, resulting in an aerosol flow rate of about 65 cc/min. The settings have to be adjusted so no error messages appear on the UCPC.

2.3.4 Atmospheric Pressure Interface Time-of-Flight Mass Spectrometer

The mass spectrometric measurements conducted in this thesis were done using an ioniAPi-ToF MS as recently introduced and described [Leiminger et al., 2019]. In general, atmospheric pressure mass spectrometry leads back to the introduction of the APi-TOF by Junninen et al. (2010). A short introduction to atmospheric pressure mass spectrometry and the differences between the originally described APi-TOF [Junninen et al., 2010] and the used ioniAPi-ToF [Leiminger et al., 2019] will be given below.
Apart from several pumps (not depicted in Figure 10), needed to create low pressures in the atmospheric pressure interface (APi) between 10^{-3} to $10-4$ mBar in order to adapt the pressure between atmospheric pressures and the 10^{-6} mBar inside the Time-of-Flight mass spectrometer (ToF), an APi-ToF consists of mainly two components: an atmospheric pressure interface and a Time-of-Flight mass spectrometer. Prior to the APi a laminar flow inlet draws aerosol at adjustable flow rates between 1 to 15 L/min. The APi consists of three individual seperate pressure stages, each containing lower pressure than the previous stage. The first two pressure stages contain identical hexapole ion guides focusing the ions in path while switching voltages and running at different frequency and amplitude settings. The hexapoles of the ioniAPi-ToF transmit a larger mass range in comparison to the previously used quadrupoles in the original APi-TOF as described recently in Junninen et al. (2010) [Leiminger et al., 2019]. The pressure in the first stage is held at roughly 2.3 mbar, in the second region it is already down to some 10^{-3} mbar. The final pressure stage of the APi, held at roughly 10^{-4} mbar, contains an ion optical lens system focusing the incoming ion beam and leading it to the ToF. The ToF itself is down to pressures at around 10^{-6} mbar. These low pressures ensure that the ions/air molecules are reduced and therefore lead to less unwanted collisions. Ions then encounter the extraction region, where the ions are pulsed away in bundles. The frequency at which these pulses occur can be varied, leading to variation in the mass range. Depending on an ion's inertia and mass/charge ratio it will have different flight times passing through the reflectron before being detected on a multichannel

plate (MCP) stack. The ions travel in a V-shaped flight path as depicted by the massive grey "V" in Figure 10. The resulting mass spectra, which give the mass-to-charge (m/z) ratio, are given in units of Thomson [Th] or, assuming z=1, in atomic mass units [amu].

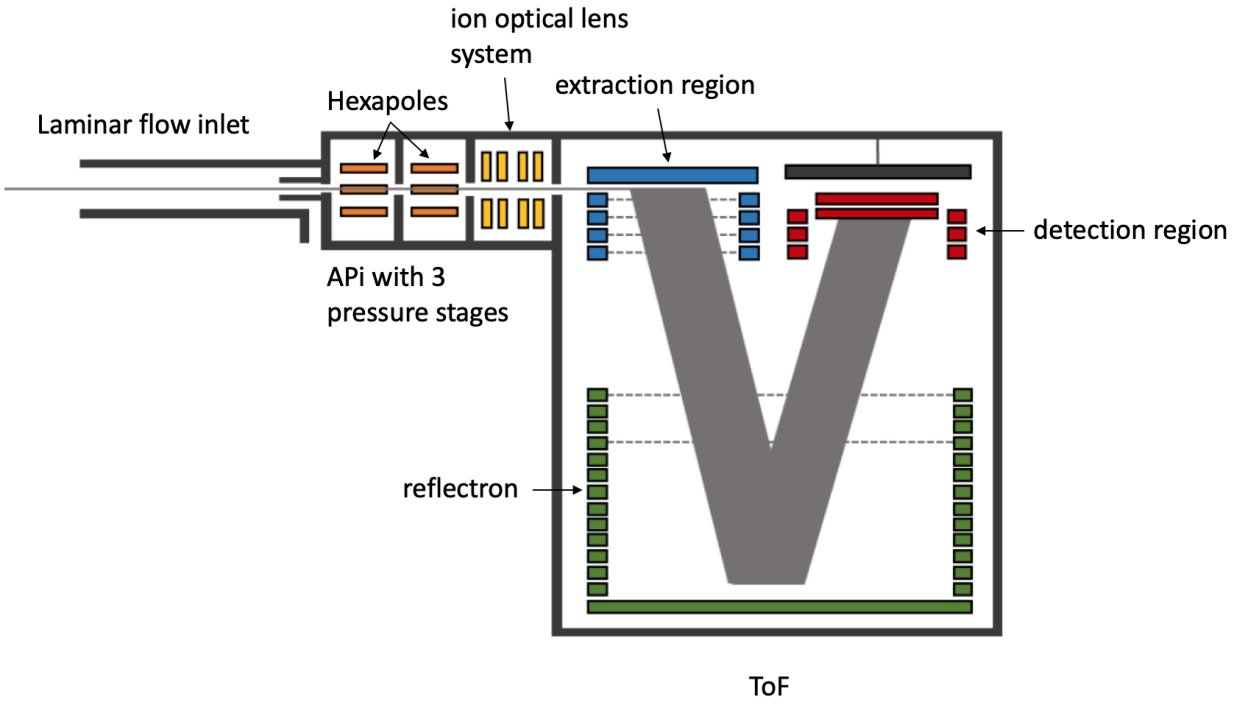

Figure 10: Schematic of the ioniAPi-ToF. The hexapoles are displayed in orange, the ion optical lens system in the last pressure stage given in yellow, the extraction region given in blue, the reflectron in green and the detection region with post acceleration and a multichannel plate (MCP) colored in red. Image taken from [Leiminger et al., 2019] and labeled according to the text.

2.3.5 Faraday Cup Electrometer

A Faraday Cup Electrometer (FCE) has the advantage of measuring particles independent of their size but solely accounting for their charge [Winklmayr et al., 1991]. This is especially useful for the characterization of CPCs and their corresponding cut-off diameters because this is a size independent measurement. A FCE consists of some type of housing acting as a Faraday cage, an electrometer to measure the current and a filter. When a charged particle enters the FCE, the charge carried by the particle induces an equal charge in the cage in order to isolate the electric field inside of it. An electrometer then measures the resulting current, which is proportional to the particle number concentration of the aerosol. The particle number concentration in FCEs is calculated according to equation (12):

$$N_{FCE} = \frac{I}{e \cdot n_p \cdot Q_{FCE}}, \tag{12}$$

where I is the electrical current, e the elementary unit of charge, n_p the number of charges per particle and Q_{FCE} the flowrate of the FCE.
A schematic of the FCE is given in Figure 11. For the measurements conducted during these experiments a University of Vienna custom built fast FCE with a response time of 0.1s as recently mentioned in Steiner (2011) was used. Originally this FCE was described in Winklmayr et al. (1991).
Measuring multiple charges on particles leads to over-counting in the FCE. Also small deviations in the current measured by the electrometer cause a fluctuation in the resulting current, therefore FCEs should regularly be off-set by measuring clean air and only measurements with a sufficient Signal over Noise ratio should be considered (in this study only particle number concentrations of roughly $>1000\text{cm}^{-3}$ were accounted for).

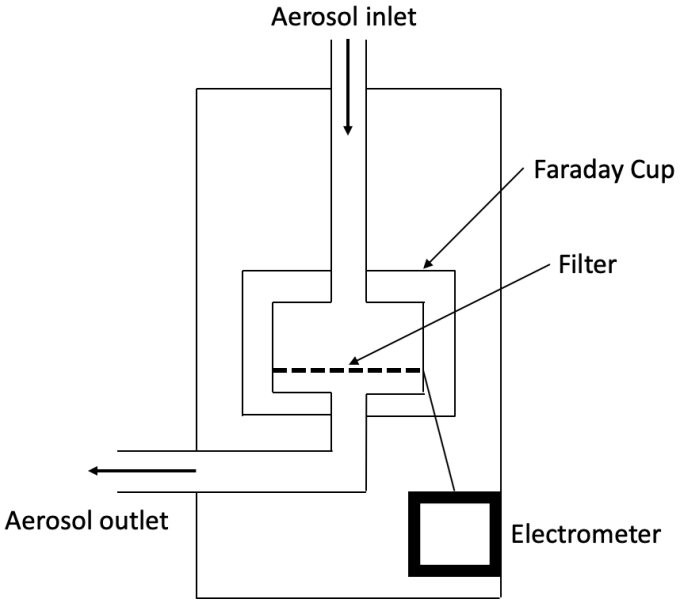

Figure 11: Schematic of a Faraday Cup Electrometer, containing an Aerosol inlet and outlet, the Faraday Cup, an Electrometer and a Filter. According to Intra and Tippayawong (2009, 2015).

3 Aim of the Thesis

Electrospraying tetra-alkyl ammonium halides has been a useful method for the generation of sub-2nm mobility standards [Ude and Fernández de la Mora, 2005, Fernandez de la Mora et al., 2005, Jiang et al., 2011]. The limiting factor in extending this size range beyond the first few clusters has been the presence of multiply charged higher clusters, which then cannot be resolved by electrical mobility anymore [Attoui et al., 2013].
With the introduction of the bipolar electrospray source a successful charge reduction mechanism for electrosprays was developed [Fernandez de la Mora and Barrios-Collado, 2017]. The aim of this thesis was to characterize such a bipolar electrospray source in regard to electrical mobility and chemical composition of the produced clusters in order to extend the size range of available monodisperse particle standards. The electrical mobility measurements were performed using an UDMA [Steiner et al., 2010] and the composition of the clusters was further investigated using an ioniAPi-ToF (ioniAPi-ToF MS, Ionicon Analytik GmbH, Austria). The electrospray was tested using solutions of THABr and TBAI dissolved in acetonitrile. After testing various settings at which the electrospray can be run, in unipolar as well as bipolar mode, several additional measurements were conducted. These included the characterization of a "tuned" TSI Model 3776 UCPC (TSI inc., Minneapolis, USA), coming up with a correct background measurement technique for mentioned characterization and the investigation of the exact cluster mass of the different higher order complex clusters corresponding to the different mobility peaks. This work was done in close collaboration with Sophia Brilke and was partly published by Brilke et al. (2020).

4 Experimental Setup and Measurement Methods

4.1 Measurement Methods and Operating Manual

This section describes how the measurements were conducted and additionally provides a detailed operating manual for the everyday lab routine.
There are different variables which can be modified to change the measurements. First of all the voltage applied to the electrospray source can either be switched on for one polarity or for both positive and negative polarities. Further, the applied voltage can be varied leading to differences in the produced signal. The applied pressure to the ES through the syringe pumps can also be modified and is monitored by a connected manometer. Next the UDMA can either be run in "scanning" mode or in "classify" mode, former meaning that the voltage is not set to a single value but scans through a previously set range of voltages, giving a complete mobility spectrum. To calibrate counters the voltage is set to a constant value ("classify" mode), resulting in a monodisperse aerosol leaving the UDMA.

4.1.1 Guide on Running the Measurements with the Bipolar Electrospray in this Setup

A step by step operating manual for measurements with the bipolar electrospray used in combination with the explained setup is given, including cleaning procedures and the necessary actions in order to perform these measurements properly. After setup installation, an experiment using the bipolar electrospray source is prepared as followed:

Turning on the Instruments:
All instruments should be turned on in time before the measurements are started. Before switching on the CPC and ioniAPi-ToF pumps it should be checked that no inlets are closed to prevent unwanted vacuum inside the systems.

- Turn on the compressed air at 2 Bar to ensure high enough flow at the electrospray chamber is provided.
- Turn on the FCE pump which is attached to the UDMA4 rack.
- Turn on the UDMA4 fan for cooling the blower.
- Turn on the UDMA4 blower with the control laptop.
- Start the UDMA4 DAQ Software "DC10DAQCPFnegV" (for negative voltage) or "DC10DAQCPFposV" (positive voltage).
- Turn on the external pumps used for the measurement devices (if necessary).
- Take off the ioniAPi-ToF inlet cap (connected to prevent contamination when not in use) and then turn on the ioniAPi-ToF stroll pump.

- Turn on the CPC or other measurement devices.
- Start all software used for data acquisition. "Aerosol Instrument Manager" for the CPC and "PTR MS Viewer" for the ioniAPi-ToF.
- While letting air run through the system to flush it with dry air, start with the cleaning process for the bipolar electrospray source.

Cleaning the Bipolar Electrospray Source before Measurements:
Cleaning the electrospray prior to any measurement is inevitable, due to capillaries tending to clog or unwanted substances in the system from previous measurements. If the electrospray is not cleaned properly the resulting signal will not be stable or no mobility spectrum at all can be obtained.

- Prepare little vials (Eppis) - 8 containing ethanol, 2 empty ones and 2 containing the solution used for further measurements.
- All further steps have to be done for both polarities:
- Attach Eppi containing ethanol without applying pressure through syringe to clean the electrode and the capillary from the outside, let it rest for 15-30 seconds before dismounting - repeat this twice. Make sure the Eppis are screwed on tightly for all further steps - this will secure a more constant pressure in the system.
- Attach Eppi containing ethanol and apply approximately -250mBar negative pressure with the syringe until bubbles start coming out of the capillary. If no bubbles appear the capillary might be clogged. To unclog the capillary either apply more negative pressure or flush the capillary by applying positive pressure followed by negative pressure until bubbles appear.
- Open syringe and attach new Eppi containing ethanol again. Apply approximately +250mBar positive pressure to the vial. Leave the system as it is for roughly 5 minutes, if the pressure drops too quickly, reapply pressure through syringes to reach 250mBar again.
- After the system is cleaned with ethanol - attach an empty vial and apply -250mBar negative pressure until little drops of ethanol come out of the capillary.
- Cleaning process is completed, the system is now ready for measurements.

Running the actual Measurements:
The goal of running the bipolar electrospray is to have two individual electrosprays of different polarities run inside the same chamber without interfering with each other. To obtain a stable signal for both electrosprays individually and running them simultaneously, several steps are necessary. Close attention should be payed to the current displayed on the electrospray source control box.

- Attach the vials containing the sample.
- Switch on the power supply for the bipolar electrospray.
- Check all aerosol flows (Electrospray, UDMA4, attached counters).
- Apply positive pressure to the bipolar electrospray source. (roughly 5-20mBar were used in the experiments performed in this thesis).
- Start the UDMA4 control software and start scanning the set voltage range.
- The two electrosprays are first turned on and adjusted individually before running in bipolar mode. To start the unipolar electrospray apply voltage to one polarity. Let it run until the current displayed on the control box of the electrospray stops fluctuating and reaches a constant value. Switch off the voltage. A representative raw unipolar mobility spectrum obtained with the FCE for THABr+ is given in Figure 12.

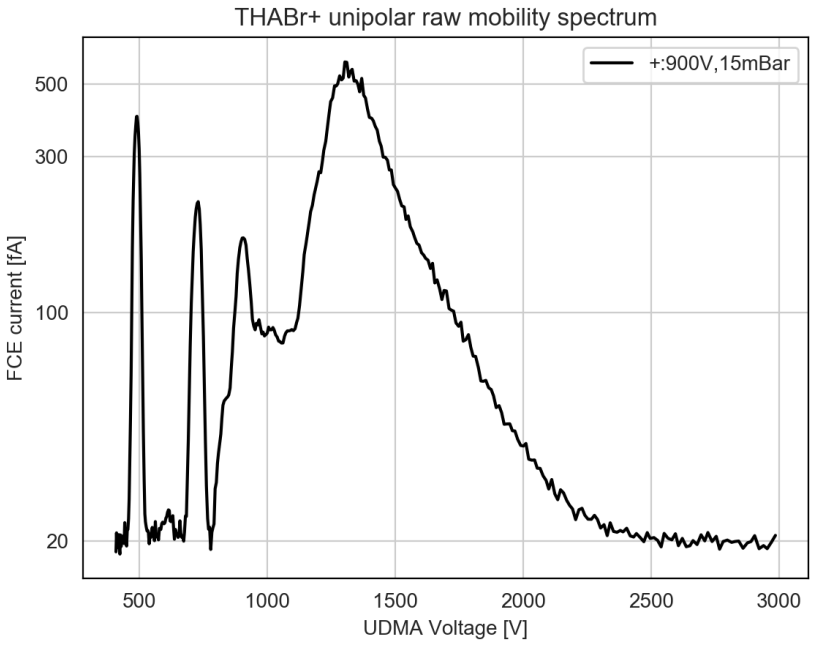

Figure 12: Raw mobility spectrum for THABr+ in unipolar mode obtained with the FCE.

- Repeat the previous step for the other polarity.
- Switch to bipolar mode by turning on the voltages for both polarities. A representative raw bipolar mobility spectrum is given in Figure 13.

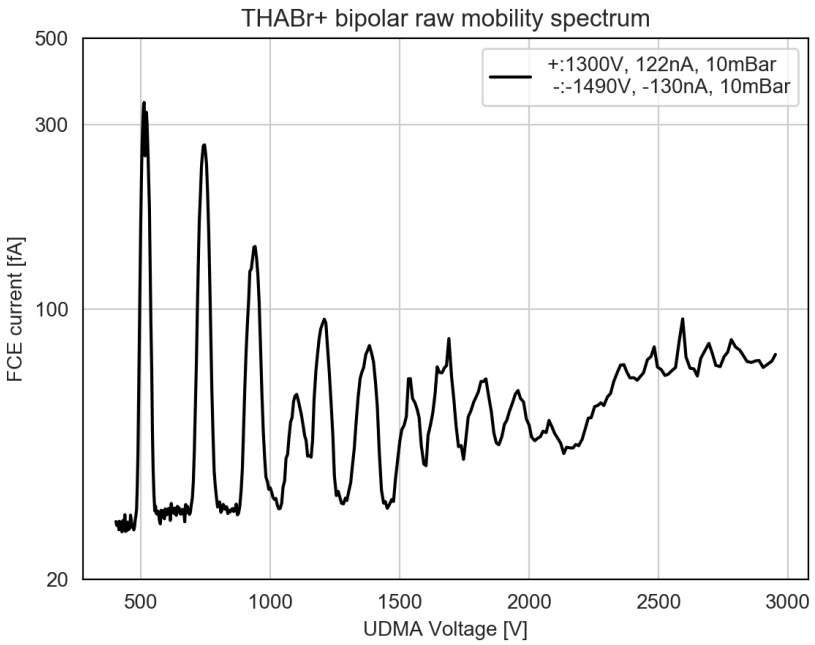

Figure 13: Raw mobility spectrum for THABr+ in bipolar mode obtained with the FCE.

- Important: the polarities should not impact each other significantly. If turning on the second polarity has a significant effect on the current of the other, it is advisable to readjust the tip position inside of the chamber in order to run the electrospray in a bipolar mode without interference caused by the opposite polarity.
- Monitor the current and wait until it stabilizes - once it has reached a constant value, the mobility spectra can be recorded and further measurements can be performed.
- Reapply pressure to the vials through the syringes in order to keep the measurement conditions stable, if necessary.

Cleaning the Bipolar Electrospray Source after Measurements:

In principle the same cleaning procedure as before starting the measurements is performed with the exception that methanol is used instead of ethanol. Therefore these steps are listed in a summarized version.

- Turn off the power supply box of the bipolar electrospray source, make sure no voltage is applied before replacing the vials!
- Attach vials containing methanol without applying pressure, rest for 15-30 seconds - repeat this twice.
- Attach vials containing methanol - apply -250 mBar negative pressure - make sure bubbles come out of the capillary.

- Attach vials containing methanol - apply +250 mBar pressure - let it rest for roughly 5 minutes.
- Attach empty vials - apply -250 mBar negative pressure and make sure little droplets of methanol come out of the capillary.
- Attach empty vials and open the syringes - the cleaning process is completed and the bipolar electrospray can be left like this until it is turned on again.

Turning off the Instruments:
Before leaving the laboratory all instruments should be switched off and checked if no pumps are creating unwanted vacuum or unnecessary contamination of the systems by running over night.

- Save all data collected.
- Close the software and shut down all laptops used.
- Turn off the CPC and all other measurement devices used.
- Turn off the external pumps.
- Turn off the ioniAPi-ToF pump and screw on the inlet cap.
- Turn off the UDMA4 blower and end the blower software.
- Turn off the FCE pump on the UDMA4 rack.
- Turn off the UDMA4 ventilator.
- Turn off the compressed air.

4.1.2 Guide for Counting Efficiency Measurements

Following steps were taken to perform an efficiency measurement while having constant electrospray signal (the necessary procedure to obtain a constant signal is described in Chapter 4.1.1):

- Set a UDMA voltage range according to the blower setting and substance used.
- Scan a complete mobility spectrum with the UDMA as seen in Figure 13.
- Select the classifier voltage equivalent to the mobility peak of the desired cluster.
- Wait until the signal stabilizes and perform a measurement over 120 seconds with the ion traps set to ground.
- For background measurements, leave the classifier voltage constant and set the voltage of the ion traps to ± 500V and perform a measurement over 120 seconds.

- Turn off the ion traps and wait for the signal to reach its original value (this may vary in time, see Figure 14).

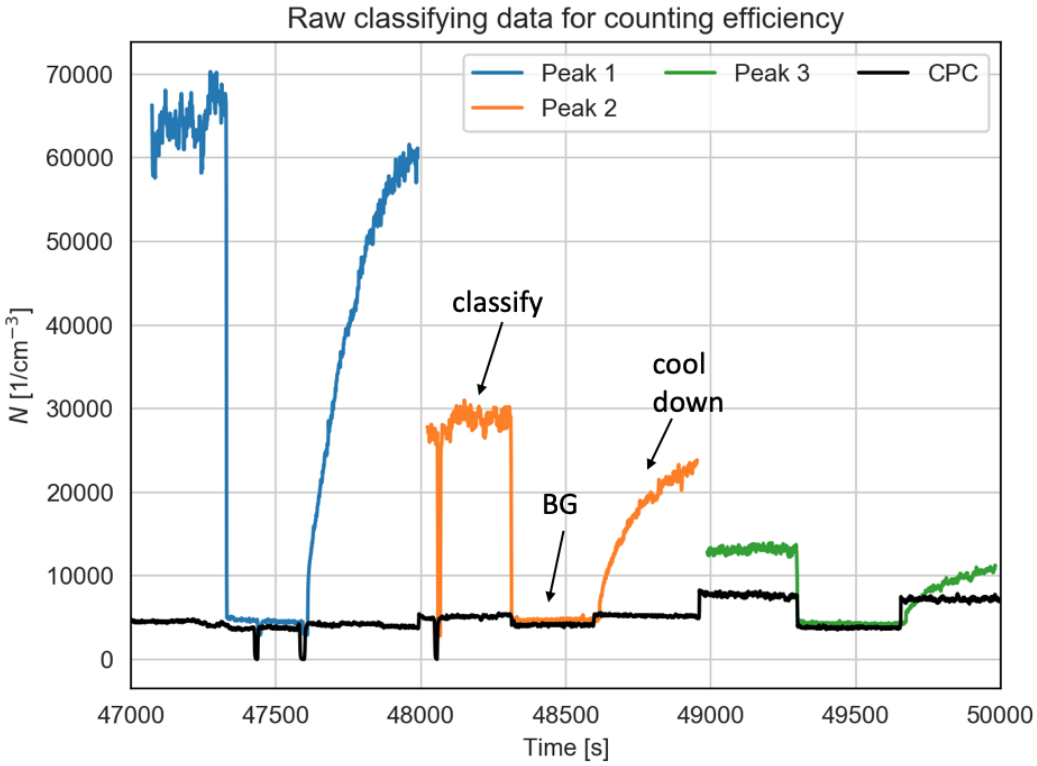

Figure 14: Example of the plotted raw data obtained by the FCE when classifying different peaks of the mobility spectrum at constant voltages and the obtained CPC data over time. The timeframes for classifying, background (BG) and "cool down" (referring to the time necessary for the signal to reach its original value due to a malfunction of one ion trap) times are labeled for the example of the dimer peak.

- Once the signal is back to original value; adjust the voltage on the UDMA to the value of the following cluster peak and repeat the previous steps. Perform this procedure for all the obtained peaks.

- If ioniAPi-ToF measurements are additionally conducted, let it record (to obtain a sufficient signal it may take up to 30 or 60 minutes depending on the order of the cluster due to low transmission in the ioniAPi-ToF for larger masses) and wait before switching the classifier voltage to the next peak. Create a new ioniAPi-ToF file for each cluster peak.

4.2 Experimental Setups

The following sub-chapters will give schematic illustrations of the different setups used during the experiments. The bipolar electrospray settings have been varied during measurements. The electrospray was either operated in uni-/or bipolar mode, switching between the two was achieved by turning on the voltages of both or only one polarity at the connected HV supply. If the UDMA was operated at high sheath air settings, then most of the time the setup given in Figure 15 was used as it included all the instruments of interest. In general, emphasis was put on keeping all sorts of tubing and distances between devices as short as possible. Additionally either stainless-steel tubing or conductive black tubing was used. All of the flows were checked multiple times during a measurement with either the Gilian Gilibrator - 2 (Serial Nr.: 1312041) or the TSI Series 4000 Flowmeter (Serial Nr.: 414006008007) and readjusted if necessary. The relative humidity in the system was also measured using SHT75 sensors with an accuracy of ±1.8% r.h. and recorded during measurements. Since it was below 2% r.h. in general it will not be further mentioned or accounted for.

4.2.1 Setup used for CPC Calibration

The majority of the counting efficiency measurements conducted were done using the following two setups. In Figure 15 an aerosol flow of compressed dry air at 10 L/min guided the ions produced by the bipolar electrospray source into the UDMA4. The UDMA4 was run at blower setting 8 which is equivalent to the higher flow setting (≈ 1000 L/min). The aerosol sample flow rate was then split with a T-piece where one end was connected to the ioniAPi-ToF, while the other end was connected to a Y-splitter (the Y-splitter was also characterized in regard to equal distributions of particles/flows for both ends). After the Y-splitter identical tubing was used to lead to the ion traps and the FCE and UCPC. The ion traps were connected to a high voltage supply and were mainly used at voltages of 500V when turned on.

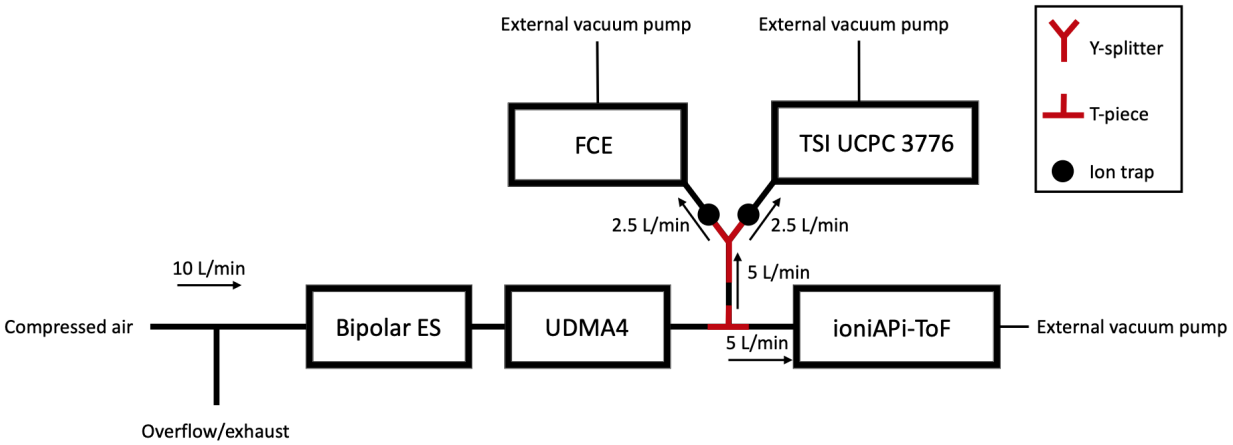

Figure 15: Schematic illustration of the Setup used for CPC counting efficiency measurements with the ioniAPi-ToF and 10 L/min aerosol flow.

The setup in Figure 16 is similar to the previous one, except for the fact that the UDMA blower was run at setting 5 corresponding to the lower flow setting ($\approx$ 400 L/min), while also reducing the aerosol flow rate to 5 L/min to maintain a Q_a to Q_{sh} ratio of roughly 1 to 10. The ioniAPi-ToF was disconnected during these measurements. The benefit of this setup was that better operating conditions for the lower blower setting were given. The setup was used for UCPC characterization measurements at lower aerosol flow rates.

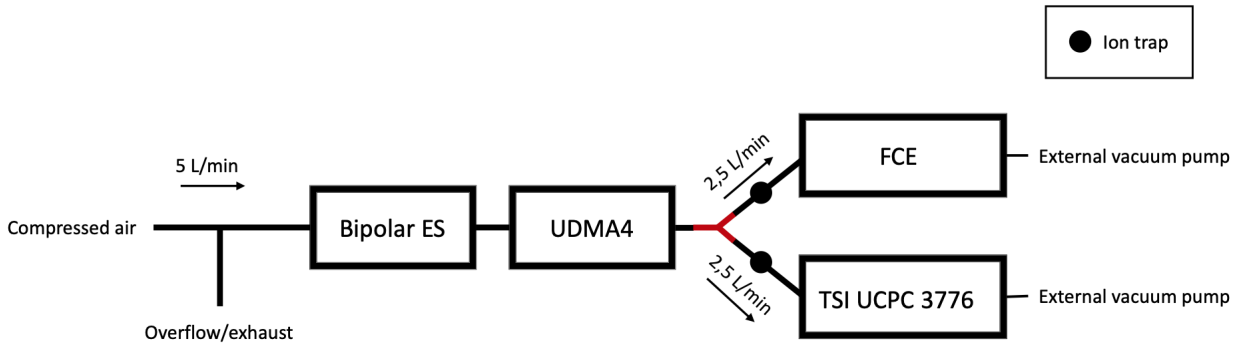

Figure 16: Schematic illustration of the Setup used for CPC counting efficiency measurements without the ioniAPi-ToF and 5 L/min aerosol flow.

As previously mentioned the TSI Model 3776 UCPC was operated at "tuned" modified temperature settings to increase the supersaturation [Barmpounis et al., 2018, Tauber et al., 2019b]. The factory settings were changed so that the temperature of the saturator, T_{sat}, was 33.1°C while the condenser temperature, T_{cond}, was set to 1.1°C. Therefore the UCPC was operated at a ΔT of 32°C. Additionally the inlet flow was raised to 2.5 L/min to minimize particle losses through diffusion.

4.2.2 Setup used for Mass Calibration and Chemical Analysis of the Clusters

The following chapter discusses the experimental setups used to record the mass spectra of the generated clusters by the electrospray. Figure 17 shows the setup for the chemical analysis of the generated clusters prior to classification. The electrospray source is directly coupled to the ioniAPi-ToF. This has the advantage that the signal intensity is generally higher than during size-resolved measurements. Since no classification of the clusters can be performed using this setup, the total mass spectrum is monitored. To obtain the full raw mass spectrum of the signal produced by the electrospray source a flow rate of 10 L/min was drawn through the bipolar ES by the ioniAPi-ToF. The ES was turned on in unipolar or bipolar mode, enabling the measurement of the full raw spectrum for both settings.

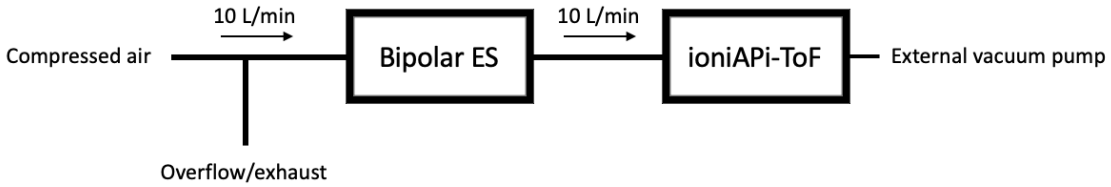

Figure 17: Schematic illustration of the Setup used to obtain the full unipolar and bipolar mass spectra with the ioniAPi-ToF.

Further mass calibration measurements were done using the setup given in Figure 15 as explained previously. Additionally the classified clusters were analyzed for chemical composition when setting constant voltage in the UDMA4. Prior to any ioniAPi-ToF measurement the mass axis was calibrated by 2 or 3 point calibration for the mono-, di- and sometimes trimer. Using the setup displayed in Figure 15 enabled to measure counting efficiency curves for the characterization of the UCPC and additionally obtain mass spectra for the single peaks when classifying a peak at a constant set UDMA voltage.

5 Data Analysis

The data analysis for the conducted measurements was separated into the analysis of the counters and the analysis of the ioniAPi-ToF. The counters record data in separate files, containing a timestamp and the corresponding particle number concentrations measured. The FCE data additionally contains a value for the applied voltage to the UDMA4 when operating it with the control box built into the rack. The ioniAPi-ToF on the other hand saves its data in the form of the mass/charge bins in a .h5 data format with corresponding counts per second values.

5.1 Raw Data

The raw mobility spectra as seen in Figure 12 and 13 present the mobility spectrum for THABr+ in unipolar and bipolar mode obtained with the FCE. The peaks in the mobility spectrum each represent the mobility of a singly charged THABr+ cluster, starting with the monomer, the dimer, the trimer, and so on. The voltage values have to be converted into inverse electrical mobility or mobility equivalent diameter values, depending on the desired final graph. The UCPC measures 10 values of counts per second and averages over these to convert it into the particle number concentration N_{CPC}. The FCE signal is obtained according to equation (12) and is calculated automatically by the software and saved as particle number concentration, for each classified peak a separate data file is obtained. The raw FCE particle number concentration has to be multiplied by a factor of $(10.2/Q_{FCE})$ due to an error in the UDMA4 software. Figure 14 shows an example of the data used to calculate counting efficiencies, in this particular case only the first three peaks and the CPC signal are plotted against time.

A python code was written and used to divide the time series into different timeframes of "classifying" and "background" (ion traps off and ion traps on with 500V applied) measurements. Each of these timeframes is then averaged over two minutes resulting in a single value for each of the classified and the background timeframes. After the background measurement a cool down time was given until the signal reached its original value, this "cool down" time was due to a malfunction in one of the original ion traps, in subsequent measurements this error was fixed and no "cool down" time was necessary. The corresponding background signal was then subtracted from the classified peak average. These resulting values for both the FCE and CPC were used to obtain the counting efficiency for each peak using equation (10).

The mass spectrum as mentioned earlier is obtained in the form of a raw signal to its mass over charge ratio. An example of a representative bipolar THABr+ raw spectrum is displayed in Figure 18. For further analysis the signal was normalized to the corresponding monomer signal or when classifying, the signal corresponding to the peak that is classified.

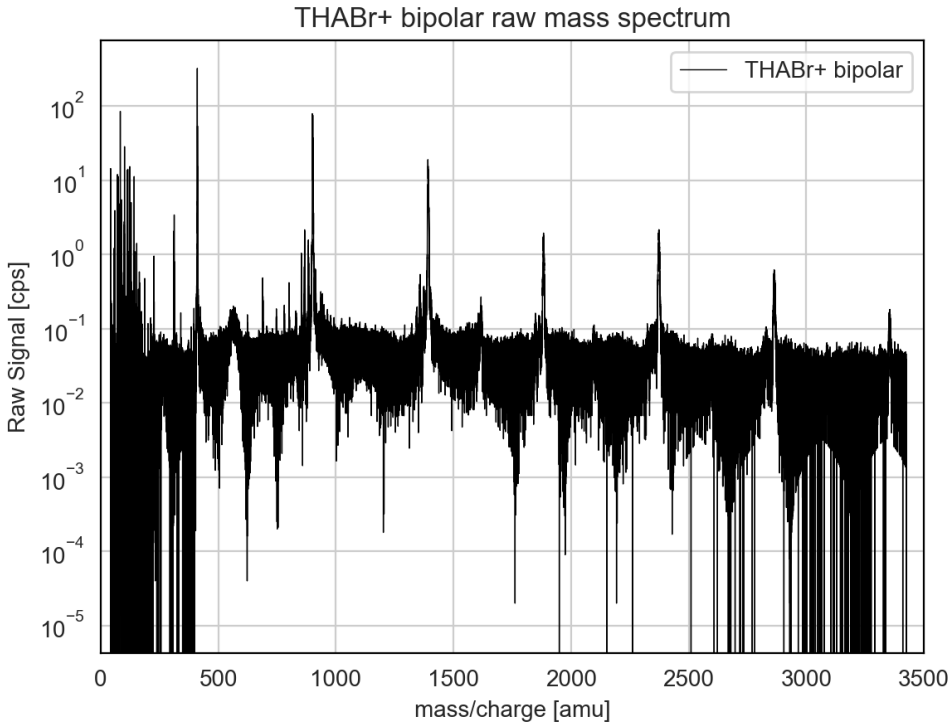

Figure 18: Example of a raw mass spectrum obtained with THABr+ in bipolar mode. The raw signal is given in counts per second [cps].

5.2 Stability of the Electrospray Source

To demonstrate the stability of the bipolar electrospray source, Figure 19 presents classifying measurements conducted over several hours. To obtain such a stable signal over longer time periods only slight pressure adjustments were necessary. The strong fluctuations in the signal at around 50000 and 55000 seconds (time of the day) represent mobility scans done before switching voltages and classifying another mobility peak. Classifying measurements over longer periods of time, as given here, were necessary to obtain mass spectra as later presented in section 6.2 THABr Characterization.

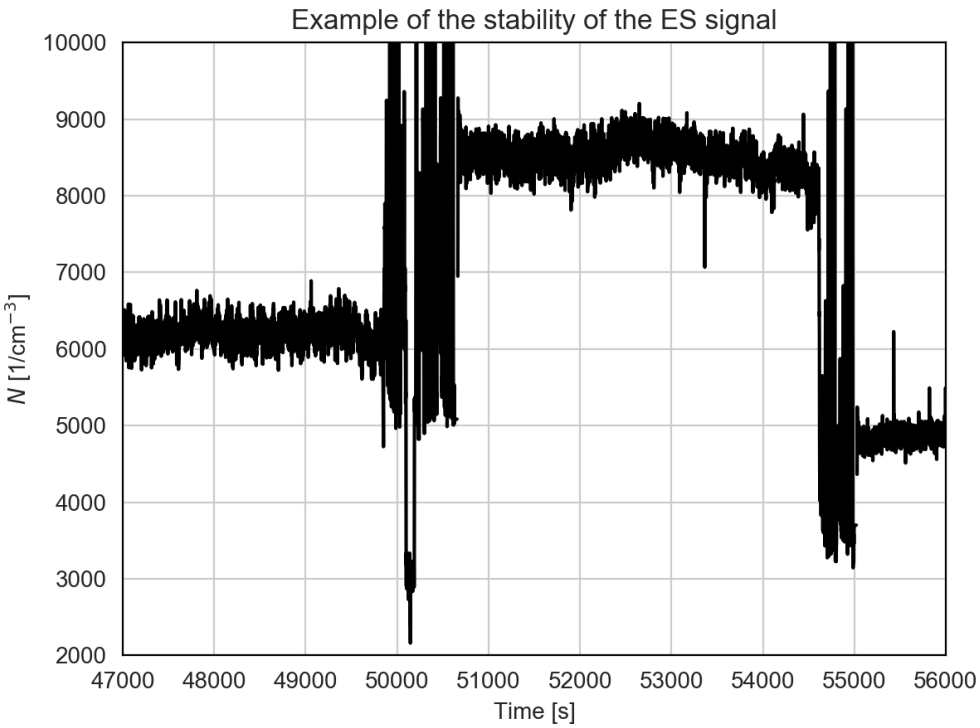

Figure 19: This plot emphasizes the stability of the bipolar ES signal. The signal was stable for roughly 150 minutes, the strong fluctuations around 50000 and 55000 seconds correspond to scans done before classifying another mobility peak.

5.3 Uncertainties

The uncertainties of experimental data is usually calculated by taking the standard deviation of the averaged mean values or gaussian error propagation. In the frame of this work the uncertainties obtained using the standard deviation of the mean signal were lower than the systematic error assigned to the instrument errors. The instrument errors effect the values of the particle number concentration obtained by the UCPC and the fast response FCE or their ratio (efficiency). The uncertainties are 10% for the UCPC [TSI, 2019] and 5% for the FCE due to uncertainties within the small currents measured and the flows. So the uncertainty for the counting efficiency adds up to 15%. Additionally the uncertainty regarding the UDMA4s resolution has to be calculated according to the method described in Flagan (1999), this impacts the calculated mobility equivalent diameter. The uncertainty of d_p is calculated for the example of the THABr+ monomer when running the UDMA4 at a resolution power of 20 and is presented in equation (13):

$$Error_x[nm] = (\frac{1}{2 * R_F}) \cdot d_p[nm] = 0.025 \cdot 1.45[nm] = \pm 0.036nm. \tag{13}$$

A gaussian curve is fitted through the monomer peak to obtain the parameters for the FWHM and position of the peak, using these values R_F is calculated.

6 Results and Discussion

This following section contains mobility and mass spectra recorded by the FCE and the ioniAPi-Tof obtained through unipolar and bipolar operation mode of the electrospray source and characterizations of settings and instruments used in the setups. Additionally, a cut-off curve for the TSI Model 3776 UCPC is presented. Furthermore, the presented results will be interpreted and discussed. For readability of the graphs the error-bars are removed on most of the presented results. Only representative results are given, even though the reproducibility was ensured. As most of the measurements done for this thesis were done using THABr, emphasis in the result section will be put on this particular substance.

6.1 Device Characterization

A characterization of the UDMA4s resolution and voltage-mobility in regard to different sheath flow rates was performed (see Table 2 and 3). To exclude measurement errors caused by unequal distribution of particles or flows to the different counters connected, a characterization of the Y-splitter was included. The characterization of the Y-splitter as displayed in Figure 21 was obtained by connecting two identical FCEs to the ends of the splitter (see setup displayed in Figure 20). The FCE inlet flow was set to 2.5 L/min for both FCEs, and the positioning of the FCEs was alternated, corresponding to setting 1 and setting 2. After obtaining off-sets for each FCE, different THABr peaks were classified in the UDMA and the obtained signals were averaged over time and compared to each other. The results show a general trend towards an efficiency of one (see Figure 21), which ensures an equal distribution of particles by the Y-splitter, excluding an impact of the Y-splitter on counting efficiency measurements.

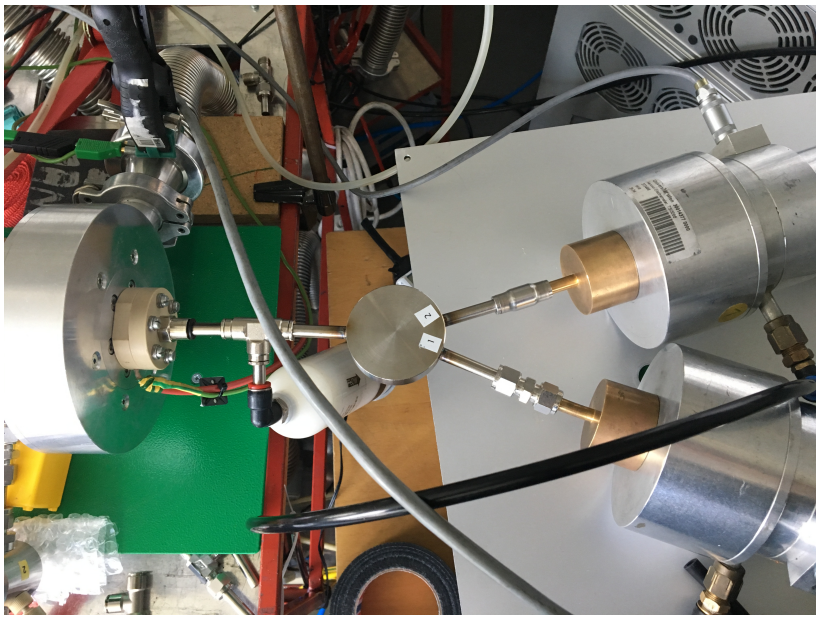

Figure 20: The UDMA4 outlet is connected to a T-piece with an overflow and to the Y-splitter with the two FCEs attached.

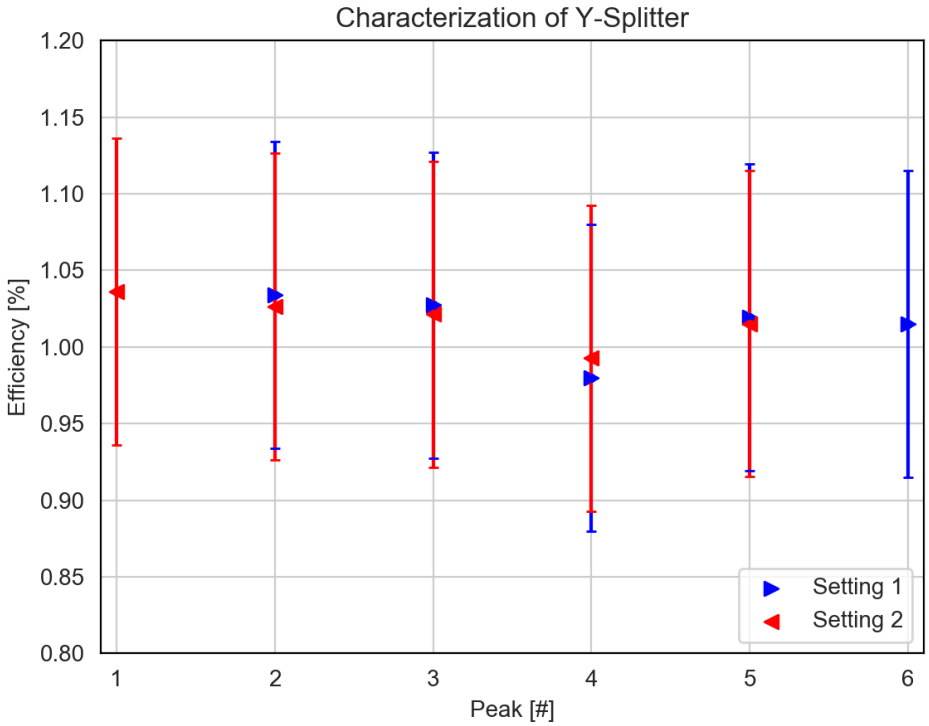

Figure 21: Characterization of the Y-Splitter used in the setup. Equal flows of 2.5 L/min were drawn through each FCE connected to the Y-Splitter. Setting 1 corresponds to the FCE1 connected to the first outlet, and FCE4 connected to the second. In setting 2 the FCEs are switched between the outlets. Different peaks of the THABr mobility spectrum were classified and the mean signal over a time period of 120 seconds of each peak was compared to determine the efficiency between the two splitter ends in regard to particle distribution.

To characterize the Q_{sh} of blower settings 5 and 8 of the UDMA4 (as described in Chapter 2.2.3) mobility spectra were evaluated. These characterizations were performed for each mobility spectrum and the average values calculated are given in Table 2.

$Q_{sh5} \approx 400$ L/min
$Q_{sh8} \approx 1000$ L/min

Table 2: Average sheath air flow rates of the UDMA4 for blower settings 5 and 8.

The Resolution Power R_F, according to Equation 7, was obtained by examining bipolar mobility spectra as seen in Figure 13 for the two different blower settings used. For the THABr+ monomer peak the resolution power (which is given as a characterization parameter for DMA's) for the two used blower settings is given in Table 3:

$R_{F5} = 17$
$R_{F8} = 20$

Table 3: Resolution power of the UDMA4 for blower settings 5 and 8.

6.1.1 Electrospray Setting Characterization

To investigate the bipolar electrospray source for different settings, measurements were conducted where multiple mobility spectra were recorded, averaged and analyzed for their corresponding peak heights (similar to the mobility spectra presented in Figures 12 and 13). The characterization of the electrospray source was performed with THABr+ for different voltages, pressures and currents applied. The results are presented (see Figures 22-24) in regard to the ratios of either the dimer or hexamer to the monomer and the height of the monomer peak signal for the different settings used. The dimer was chosen to compare between unipolar and bipolar mode, while the hexamer was chosen as a representative peak for the higher order clusters in regard to signal and stability. The characterization of the bipolar electrospray source for unipolar electrospraying of THABr+ is shown in Figure 22. The ratios of the dimer to the monomer are presented for different pressures and voltages applied. A correlation between higher voltages and higher ratios can be interpreted as a shift of the overall signal of the mobility spectra towards the dimer and additionally the multiply charged cluster signal "hill" (see Figure 12). While higher pressures lead to higher overall signal, the longevity of the stability of the signal drastically decreases due to strong pressure drops in the system, therefore leading to higher frequencies of reapplying pressure, causing instability of the signal. As a consequence the subsequent measurements were performed at pressures around 5mBar to 30mBar, putting more emphasis on the stability of the signal rather than signal height.

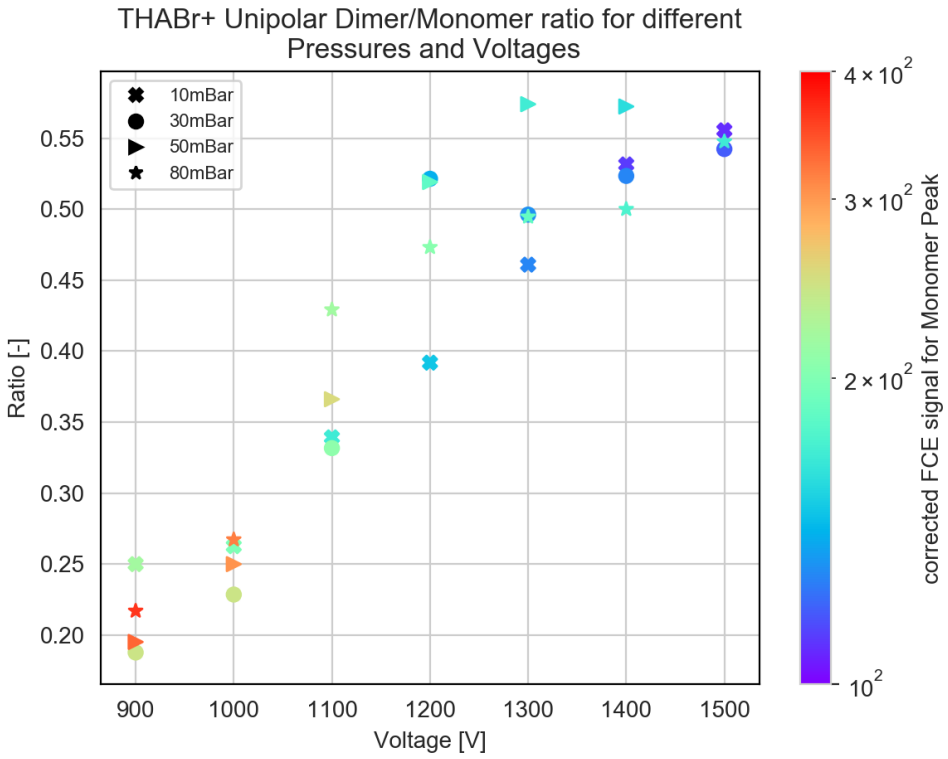

Figure 22: Ratios of the dimer to monomer signal for different pressure and voltage settings when spraying THABr+ in unipolar mode. The colorbar indicates the height of the corresponding monomer peak.

The characterization of the bipolar settings for symmetrical (same currents applied to each polarity) and asymmetrical operating conditions (higher positive (asymmetrical positive) or negative (asymmetrical negative) currents applied) are presented in Figures 23 and 24. Additionally to the unipolar analysis not only ratios of dimer to monomer are compared but also hexamer to monomer ratios, to include a higher order cluster. Due to a broken capillary tip, higher voltages had to be applied in order to maintain a Taylor Cone for one polarity, and therefore the bipolar settings were compared through electrospray currents. The broken capillary tip had a larger tip diameter compared to the non-broken other one.

For symmetrical settings (see Figure 23), results similar to unipolar mode can be observed, where higher currents, correlating to higher voltages, lead to higher ratios of the dimer/hexamer to monomer. The monomer signal increases for lower currents and decreases at higher currents. Higher ratios for higher ES currents, as previously seen in unipolar mode (see Figure 22), indicate a shift of the signal towards higher order clusters. A possible explanation for this behavior might be that the system contains more energy and therefore the higher order clusters are more likely to recombine and form singly charged clusters.

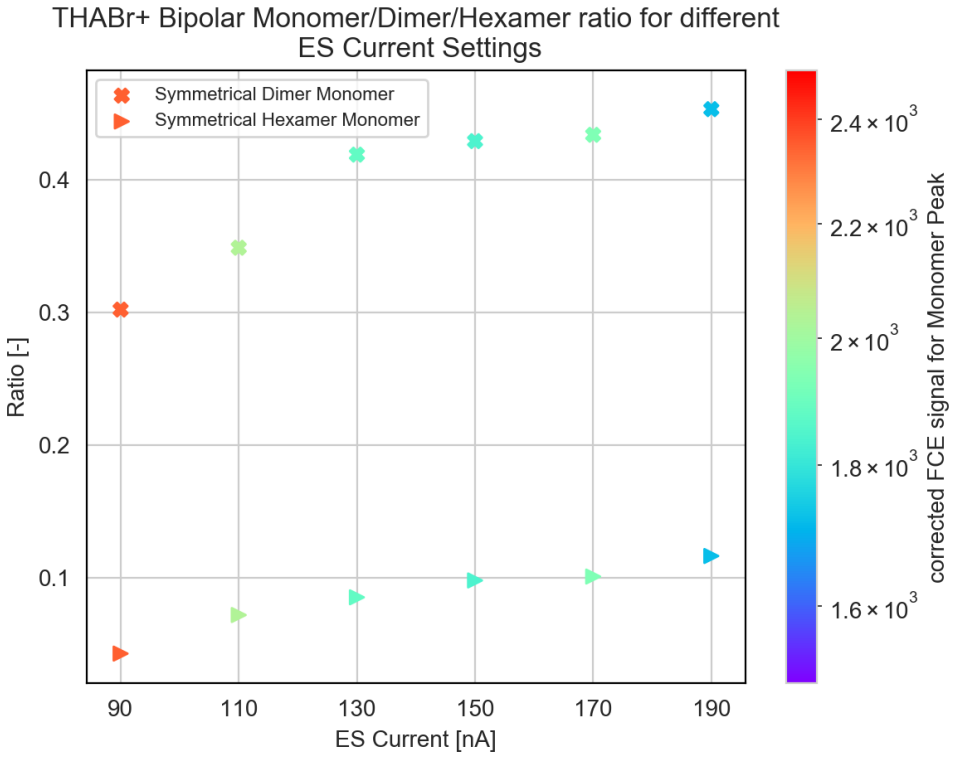

Figure 23: Ratios of the dimer and hexamer to the monomer signal for different symmetrical ES Currents spraying THABr+ in bipolar mode at 10mBar.

In Figure 24, these ratios differ in comparison to the ratios previously shown for symmetrical or unipolar settings. Focusing on the top panel of Figure 24, the overall signal of the monomer across all settings is higher compared to asymmetrical negative settings. Additionally, the ratios are comparable with the symmetrical operating conditions. The lower panel, displaying settings where the negative currents were lower, has significantly lower monomer signal but higher overall ratios. Unlike the other bipolar results no trend towards higher currents can be seen. These results led to the conclusion that symmetrical electrospray current settings were best suited for the measurements conducted in the frame of this work as they ensured a high signal for larger peaks while still enabling characterization of the sheath flow and resolution of the UDMA4 with a high enough monomer signal. These characterizations of the electrospray settings should be repeated for further substances in future work.

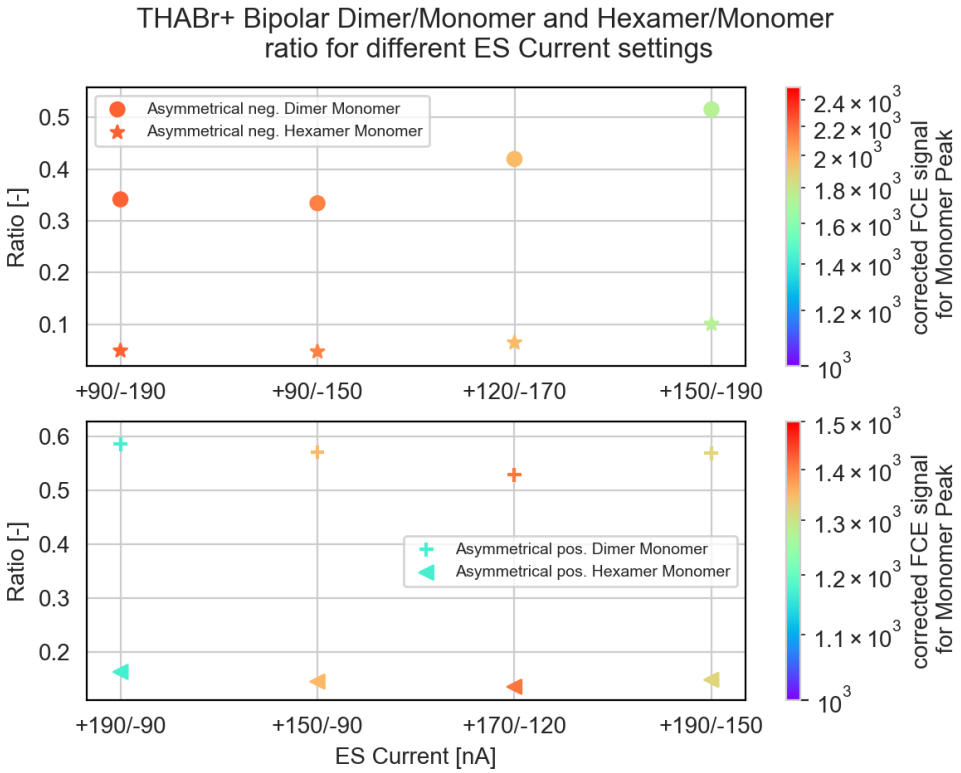

Figure 24: Ratios of the dimer and hexamer to monomer signal for different asymmetrical ES Currents spraying THABr+ in bipolar mode at 10mBar.

6.2 THABr Characterization

Positive and negative THABr clusters were investigated, to confirm that successful charge reduction can be achieved by switching from unipolar to bipolar electrospraying and that the range of mobility standards can be extended beyond previously measured sizes [Steiner et al., 2010, Attoui et al., 2013]. This following chapter presents mobility spectra for unipolar and bipolar mode recorded by the FCE, complete and classified mass spectra for individual peaks from the ioniAPi-ToF and a counting efficiency curve for the TSI Model 3776 UCPC with modified temperature settings.

6.2.1 Unipolar

In order to compare subsequent bipolar mobility measurements, unipolar mobility spectra were recorded with the same setup for both THABr± and are presented in Figures 25 and 26. These align with the mobility spectra obtained by electrosprays prior to the introduction of the bipolar electrospray [Steiner et al., 2010, Attoui et al., 2013].

The positive THABr unipolar spectrum for blower setting 5 is given in Figure 25, a clear peak for the monomer and dimer can be seen as well as a possible trimer. For inverse mobilities larger than 2 Vs/cm^2 a large "hill" of complex multiply charged clusters makes further peaks indistinguishable by mobility and therefore non viable for subsequent counting efficiency measurements with a CPC and an FCE. The multiple charges on particles lead to clusters of different sizes having the same mobility and therefore the size of the particles can not be calculated through their mobility, furthermore the multiple charges lead to the previously mentioned over counting in the FCE and therefore make counting efficiency measurements with a FCE as a reference device invalid.

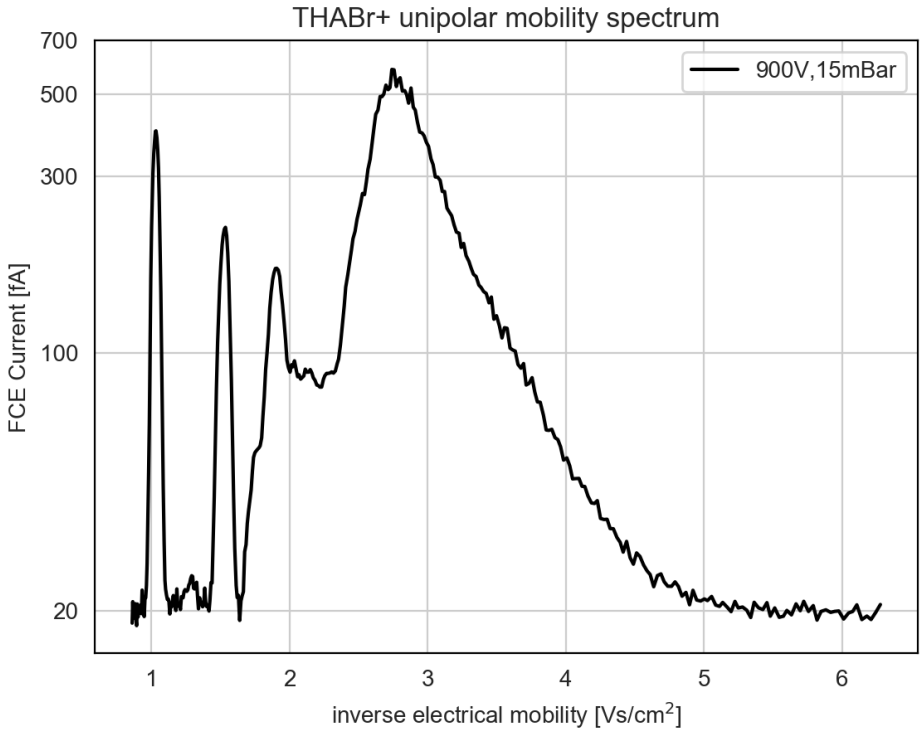

Figure 25: Unipolar mobility spectrum of THABr+ while operating the UDMA4 at blower setting 5 and the electrospray at 900V with 15mBar pressure applied.

The THABr- unipolar mobility spectrum shows similar results as the THABr+ spectrum, a clear monomer and dimer and a potential trimer are detected (see Figure 26). The signal height for the detectable peaks is significantly lower for negative clusters. For inverse mobilities larger than 1.5 Vs/cm^2 the multiply charged clusters make it impossible to distinguish different clusters by mobility in accordance to the THABr+ results.

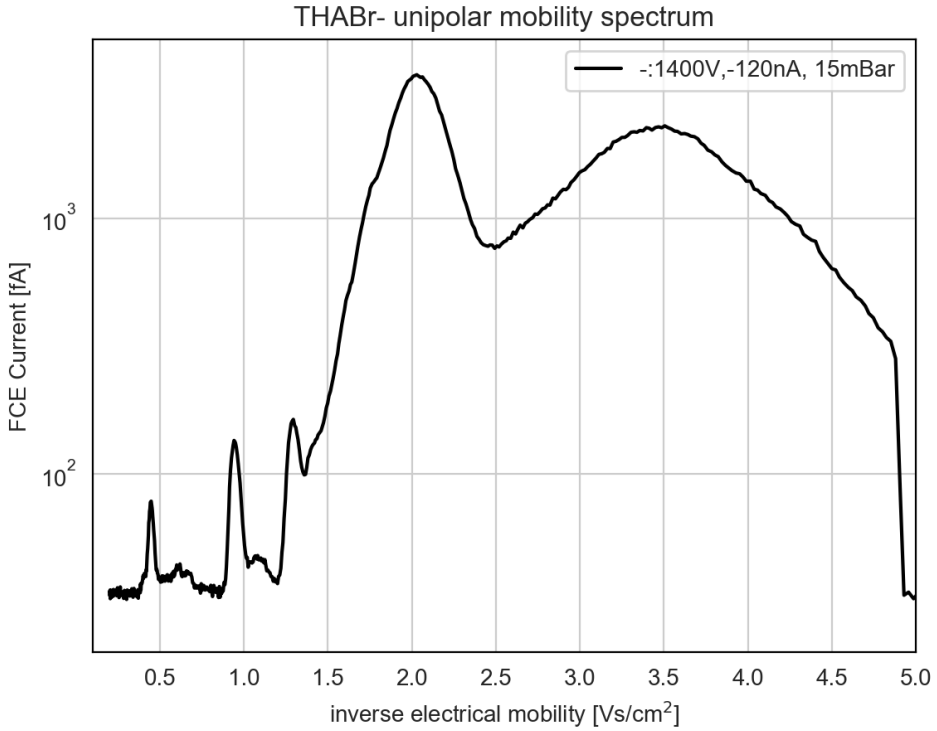

Figure 26: Unipolar mobility spectrum of THABr- while operating the UDMA4 at blower setting 5 and the electrospray at 1400V with 15mBar pressure applied.

6.2.2 Bipolar

To confirm that switching to bipolar mode for the electrospray source leads to a charge reduction and therefore extends the range of distinguishable mobility peaks [Fernandez de la Mora and Barrios-Collado, 2017], several measurements were performed. For THABr, the following Figures will show a comparison between unipolar and bipolar mobility spectra for both THABr± (Figures 27 and 29) and a bipolar spectrum with higher resolution for THABr+ (Figure 28). Additionally a chemical analysis of the sprayed signal with the ioniAPi-ToF (Figures 30 and 31) and a counting efficiency curve for the TSI Model 3776 UCPC (Figures 32 and 33) are given.

The bipolar mobility spectra recorded for THABr+ (black) shows individual mobility peaks up to n=9, each of these represent a singly charged higher order cluster. This extends the previous range given in unipolar mode n=3 (grey) significantly (see Figure 27), showing

that even for lower resolutions of blower setting 5 the individual clusters, produced with the bipolar electrospray source for THABr+ using this setup, can be resolved. The tetramer (n=3) is lower than the neighboring peaks, but still resolved as a "shoulder" peak of the pentamer (n=4), in agreement with prior observations [Ude and Fernández de la Mora, 2005, Fernandez de la Mora and Barrios-Collado, 2017]. These results were obtained with the half-mesh mounted in the electrospray chamber. Previous measurements done with the full-mesh did not resolve a tetramer (data not shown), therefore the full-mesh was excluded from further measurements based on this observation. This was in agreement with the manual of the bipolar electrospray sources manufacturer, stating that the full-mesh is preferable for spraying virus-like particles, while the half-mesh is advised for spraying salts. Subsequent higher resolution UDMA4 and ioniAPi-ToF measurements (see Figure 28 and 31) confirmed that the tetramer is indeed at the expected mobility.

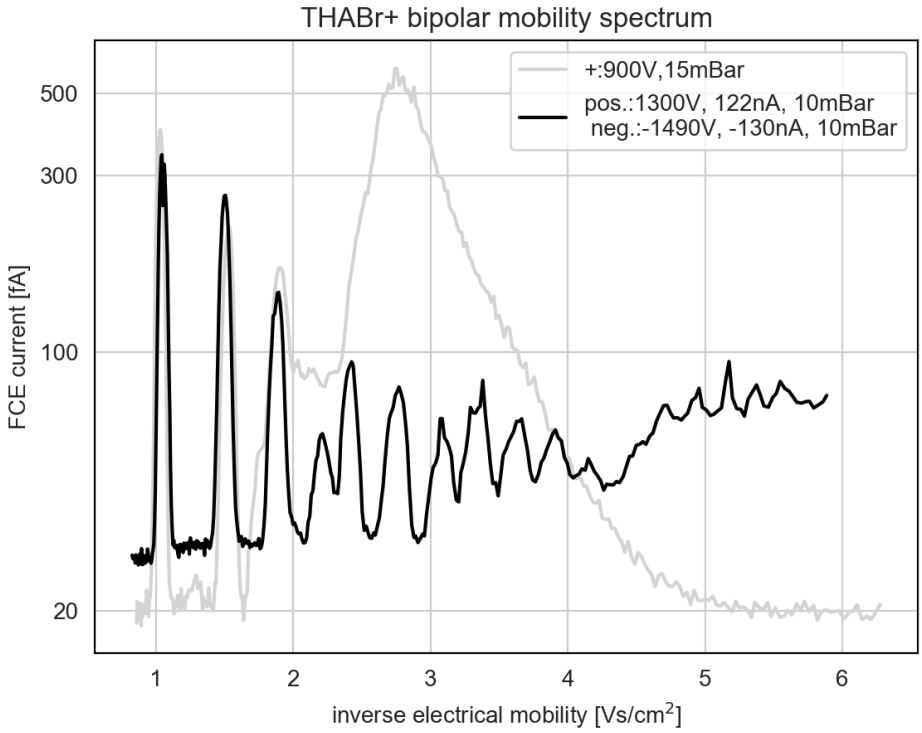

Figure 27: Overlay of the mobility spectra of THABr+ for unipolar (grey) and bipolar (black) setting of the ES with the UDMA4 blower at setting 5. The complex multiply charged clusters that build the indistinguishable signal in unipolar mode separate into distinguishable peaks in bipolar mode.

The mobility spectrum for higher resolution and symmetrical electrospray settings given in Figure 28 shows individual peaks for the first n=9 THABr+ clusters. The higher sheath air flow rate leads to a higher resolution and lower transmission for higher clusters, therefore the electrospray needed to produce a stable and high signal for further characterization measurements with these clusters. As these settings produced a stable signal, further measurements for the characterization of the clusters in the ioniAPi-ToF and counting efficiency measurements with the UCPC were performed successfully with this setup. The tetramer is resolved as an individual peak in this spectrum at a sheath air flow of 1000 L/min, and not a "shoulder" of the pentamer as in the previous spectrum. Thus confirming that the setup used with an UDMA4 is capable of detecting this cluster. The range of detectable mobility peaks could be extended by using DMAs with higher resolution as described in Fernandez de la Mora and Barrios-Collado (2017). A higher resolution power would lead to higher chemical purity of the classified clusters. The non-ideal peak shapes can be explained by deviations in the DMAs geometry, for example the UDMA4s eccentricity. Optionally a parallel plate DMA could be used due to the higher resolution powers caused by their favorable geometry.

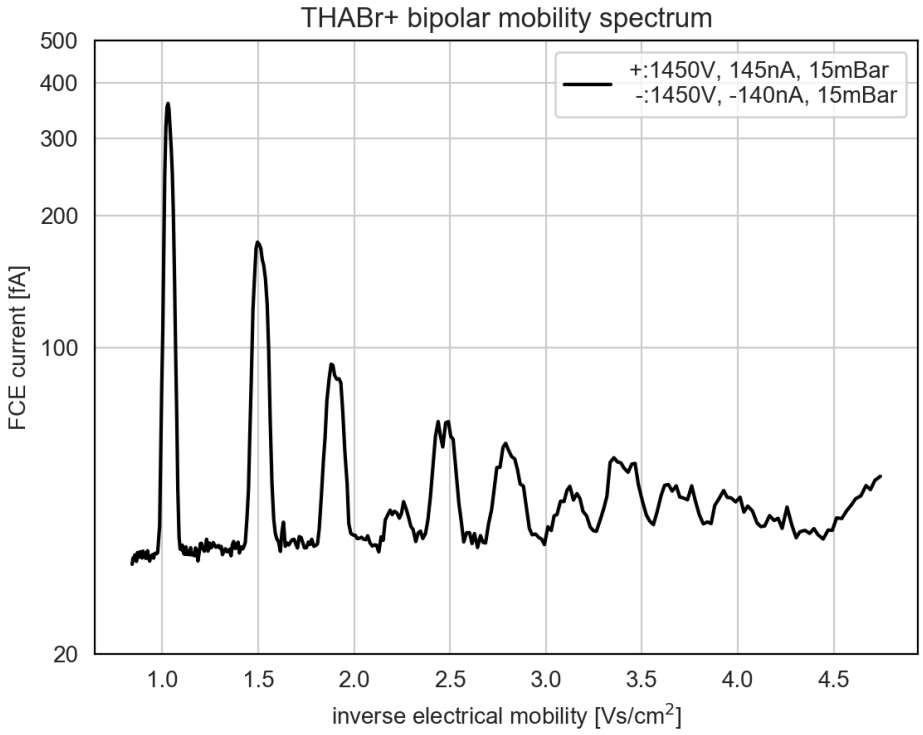

Figure 28: Bipolar mobility spectrum of THABr+ while operating the UDMA4 at blower setting 8 and the electrospray at 1450V for each polarity with 15mBar pressure applied.

To verify that the bipolar electrospray produces dominantly singly charged clusters not only for positive cluster polarity but also for THABr-, mobility spectra for negative clusters in both unipolar (grey) and bipolar (black) mode were recorded at blower setting 5 and are shown in Figure 29. The switch to bipolar mode clearly shows that the charge reduction of the higher order clusters leads to individual peaks being resolved by mobility up to n=8. The "shoulder" peaks visible for the monomer and dimer were not further identified, because their inverse mobility did not correlate to a THABr- cluster and therefore were not accounted for. These peaks are due to the "low" resolution of the UDMA4 and could be avoided by using a DMA with higher resolution and/or different geometry. Future studies have to investigate this polarity in more detail to better characterize the nature of these peaks. To resolve higher order larger clusters a DMA with higher resolution is advised [Fernandez de la Mora and Barrios-Collado, 2017], extending the range of detectable singly charger clusters for given polarity.

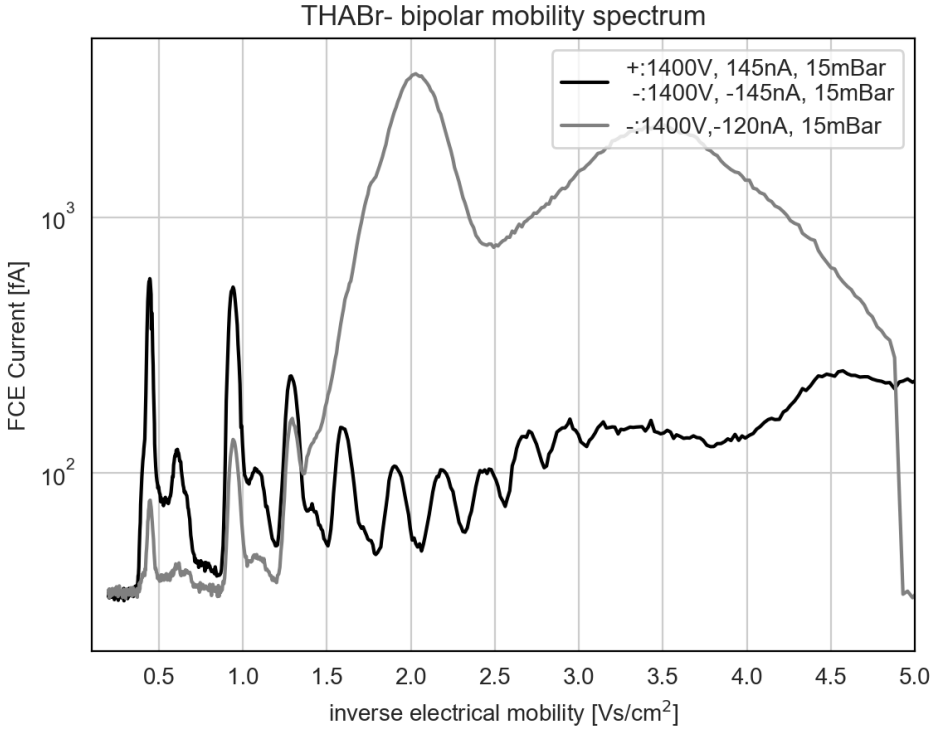

Figure 29: Overlay of the mobility spectra of THABr- for unipolar (grey) and bipolar (black) setting of the ES with the UDMA4 blower at setting 5. The complex multiply charged clusters that build the indistinguishable signal in unipolar mode separate into distinguishable peaks in bipolar mode.

Placing the bipolar electrospray source directly in front of the ioniAPi-ToF (see Figure 17), enabled obtaining complete mass spectra of THABr+ in unipolar (blue) and bipolar (red) mode without any interaction or classification in the UDMA4 and therefore largely increased transmission. These mass spectra are presented in Figure 30. Both spectra are normalized to the monomer signal for comparability and are averaged over a time of 5 minutes. The singly charged clusters up to n=6, as given in Table 1, are labeled and exist in both spectra. The grey markers indicate masses of doubly charged clusters according to Fernández de la Mora et al. (2005), the signal of these clusters is clearly reduced when switching to bipolar mode. The background noise is higher in unipolar mode and additional peaks between clusters larger than the trimer are detected. In bipolar mode the overall background signal decreases and these additional peaks between clusters seem to disappear. For smaller masses < 800 amu, several peaks show up in the bipolar spectrum, these could be associated with fragmentation in the ioniAPi-ToF. Additionally, peaks associated to water (even though the r.h. in the system was kept low, water is still present in air), acetonitrile or ethanol recombining with cluster can be observed. In general there are several uncertainties around fragmentation and transmission of mass spectrometers. The operating settings should be chosen in order to minimize fragmentation as that would lead to peaks being detected which are not present outside of the ioniAPi-ToF [Heinritzi et al., 2016, Passananti et al., 2019]. The method used with the bipolar electrospray for generating mobility standards (including the UDMA) with well known composition can also be used to characterize APi-ToFs. Enabling characterization of instrument settings to study the effect on fragmentation and transmission as well as calibrating the mass axis for larger masses. In the study of Leiminger et al. (2019) they investigated the fragmentation of well known clusters for different instrument settings. This should be kept in mind for future studies.

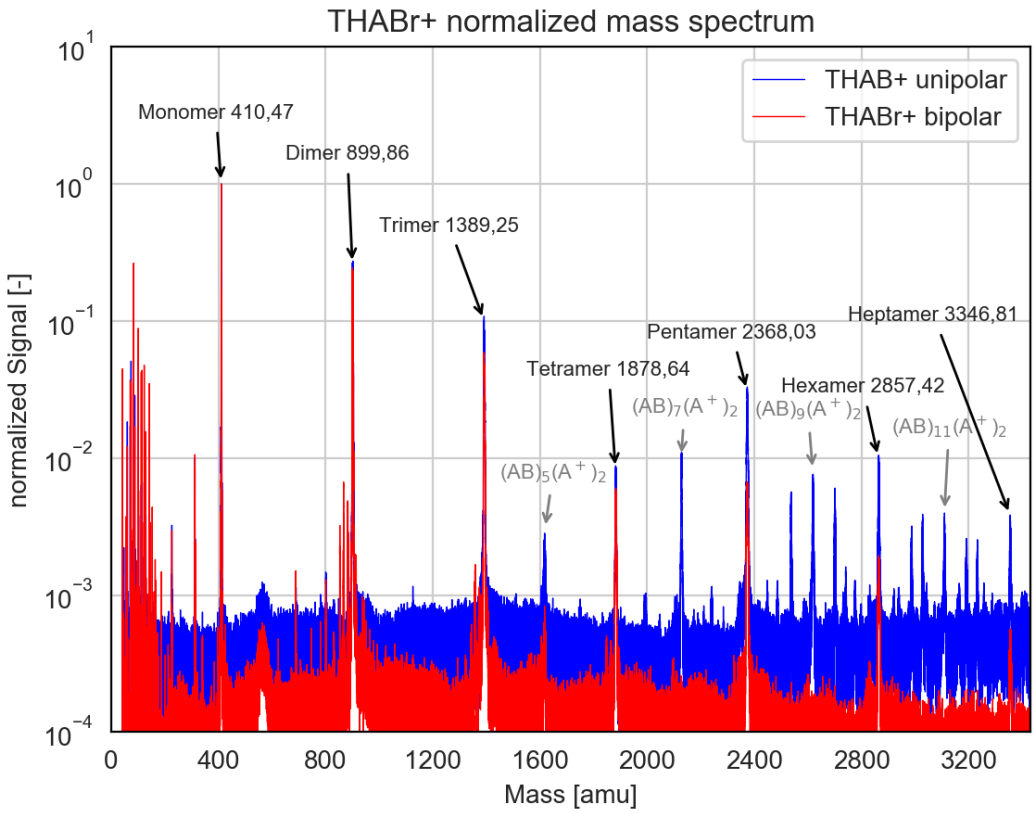

Figure 30: Mass spectrum of spraying THABr+ in uni-/ and bipolar mode obtained by using the setup given in Figure 17. The spectrum was normalized to the monomer signal. The clusters and their corresponding masses are labeled up to the heptamer (n=6). The grey markers show the doubly charged clusters as presented in Fernández de la Mora et al. (2005). The spectra were averaged over a time of 5 minutes.

Classification measurements with the ioniAPi-ToF were performed, to confirm that the mass of the classified mobility peaks corresponds to the mass of the singly charged THABr+ clusters. The UDMA4 voltage was set constant at the corresponding mobility peak and the clusters up to n=6 were classified and the spectra were normalized to the according cluster (see Figure 31). The low intensities for higher order clusters in comparison to smaller clusters is caused by the low transmission efficiency of the ioniAPi-ToF for large mass/charge ratios and their corresponding higher transmission probability in the UDMA4. To account for this the different peaks were classified for increasing time periods with increasing size of the clusters. For the monomer, dimer and trimer additional peaks can be seen in the mass spectra, these are possibly associated to fragmentation in the ioniAPi-ToF [Leiminger et al., 2019], perhaps hinting that these smaller clusters do not remain intact when transitioning from ambient to low pressures, similar observations have been made by Ude and Fernandez de la Mora (2005). The spectra show that a clear association between the mobility peaks and their expected cluster mass can be made, confirming that the classified THABr+ mobility

peaks can be assigned to their corresponding singly charged clusters.

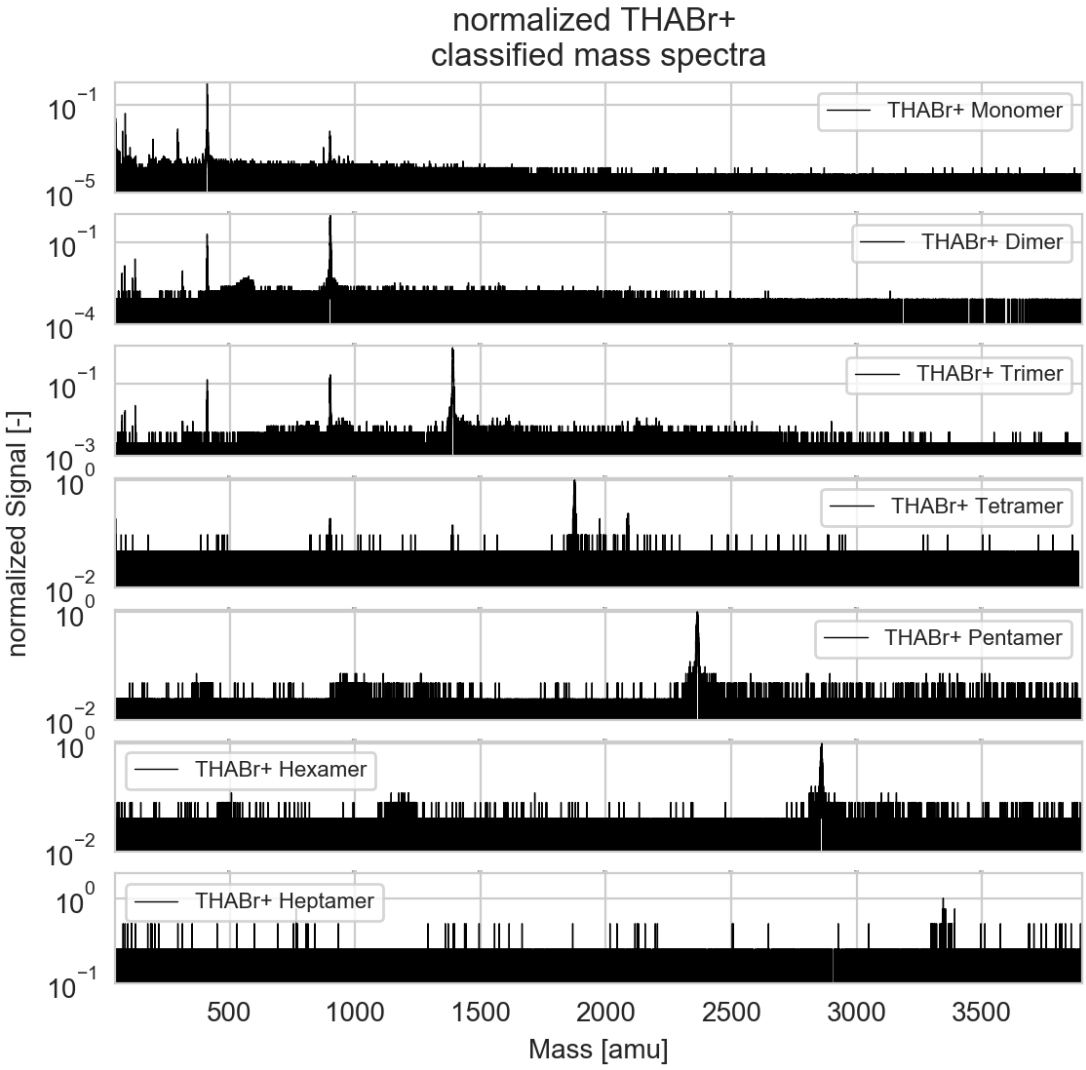

Figure 31: Mass spectra obtained by the ioniAPi-ToF for the different classified mobility peaks of THABr+ up to a cluster size of n=6. The spectra were normalized to the according classified clusters.

6.2.3 Counting Efficiency

The bipolar electrospray source in combination with this setup demonstrates that the range of accessible mobility standards can be extended and each mobility peak can be associated to the corresponding THABr+ cluster. The next step was to prove if particle counters can be characterized with this setup. Figure 32 shows a representative counting efficiency curve for the TSI Model 3776 UCPC running under higher supersaturation conditions due to alternated temperature settings as previously done by Barmpounis (2018) and an increased inlet flow in the UCPC to minimize diffusional losses with the UDMA4, demonstrating that particle counters can be characterized successfully with this setup. The first ten peaks were classified, resulting in a characterization for mobility equivalent diameter sizes up to 2.8nm. The cut-off diameter $d_{50} = 1.98 \pm 0.11$nm was calculated according to an empirical fit applied to the counting efficiency curve (see equation (14)). These results correlate with the previously measured cut-offs for this UCPC with different substances [Tauber et al., 2019a, Tauber et al., 2019b].

$$y = a * e^{-e^{-k \cdot (x - x_0)}} \cdot (1 - e^{-x \cdot n}) \tag{14}$$

Where x is the independent variable, y the value of the function at x, a is a parameter linked to the position of the plateau, k to the curvature, x_0 the offset and n the n^{th} root function. The corrected FCE signal for each mobility peak is given in the colorbar, high signal to noise ratios of the number particle concentration in the FCE were ensured throughout the measurement. The counting efficiency measurements in combination with the previously shown mass spectra further confirm that the classified mobility clusters are dominantly singly charged. The FCE only accounts for a particle's charge, therefore multiple charges would lead to over counting in the FCE and efficiencies of 1 could not be achieved.

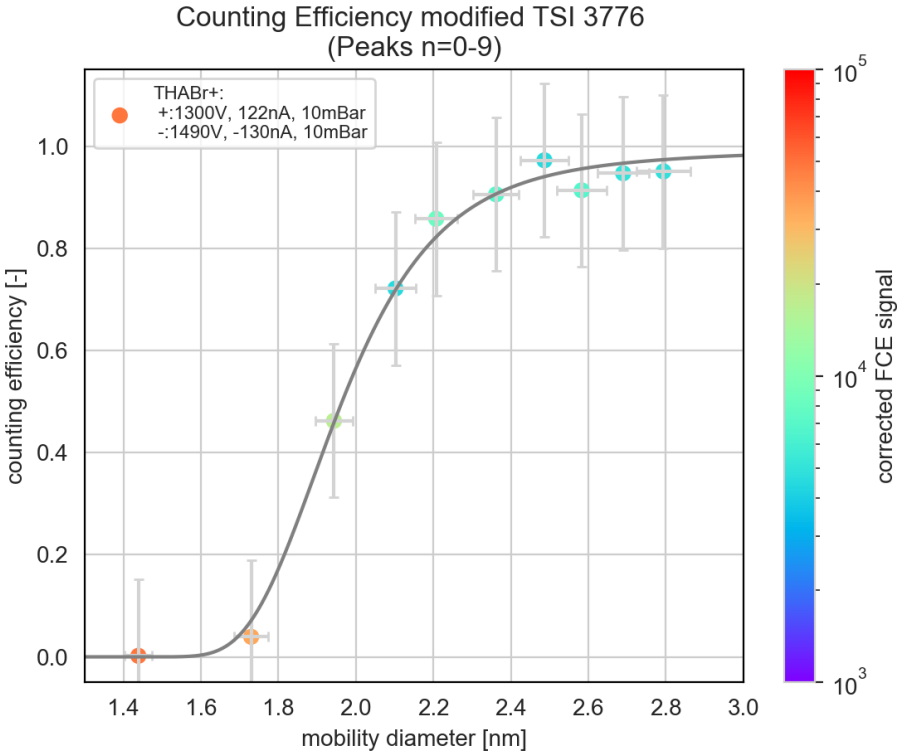

Figure 32: Plot of the counting efficiency of the TSI Model 3776 UCPC for THABr+ for the first ten peaks, the corrected FCE signal for each peak is given in the colorbar. The cut-off diameter is d_{50}=1.98±0.06nm. An empirical fit is applied to the curve and displayed as the grey curve.

A THABr+ mobility spectrum in regard to mobility diameter (see equation (4)) and the corresponding counting efficiency curve is presented in Figure 33. Under the conditions displayed in Figure 32 the bipolar electrospray source produces mobility standards in the size range of 1.45-2.8nm, which can successfully be used to characterize the size range surrounding the cut-off diameter of a TSI Model 3776 UCPC.

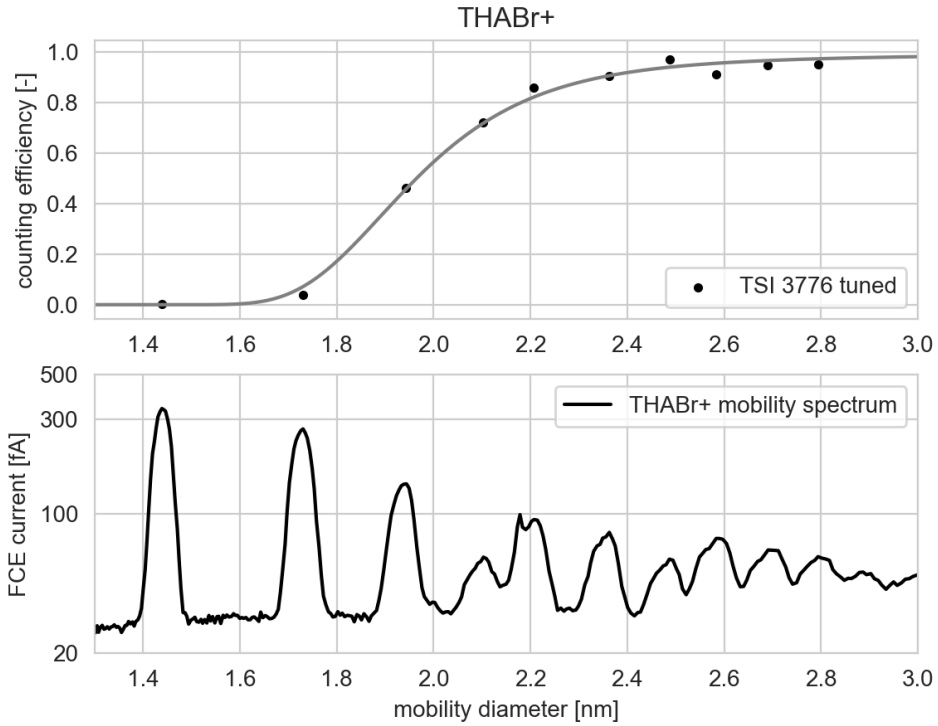

Figure 33: Plot of the bipolar mobility spectrum for THABr+ along with the corresponding counting efficiency curve for the TSI Model 3776 UCPC. The cut-off diameter is d_{50}=1.98±0.06nm. An empirical fit (grey) is applied to the curve.

6.3 TBAI and TMAI Characterization

Additional experiments were performed with two further commonly used tetra-alkyl ammonium halides [Ude and Fernández de la Mora, 2005, Steiner et al., 2010, Heinritzi et al., 2016], namely TBAI and TMAI (see Chapter 2.1.3), to confirm that the results obtained by this setup for THABr can be verified for further substances. Since the main focus of this thesis was put on THABr, these additional substances were not characterized as detailed. This chapter will present unipolar and bipolar mobility spectra of TBAI+, a bipolar mobility spectrum for TBAI- and complete mass spectrum of TBAI+ as well as TMAI+.

6.3.1 Unipolar

Similar to the THABr+ unipolar spectrum (see Figure 25), the unipolar TBAI+ mobility spectrum in Figure 35 shows a clear monomer, dimer and a trimer. For inverse electrical mobilities >1.5 Vs/cm^2, the clusters can not be separated by electrical mobility. In the unipolar results only a positive mobility spectrum for TBAI is presented in this work.

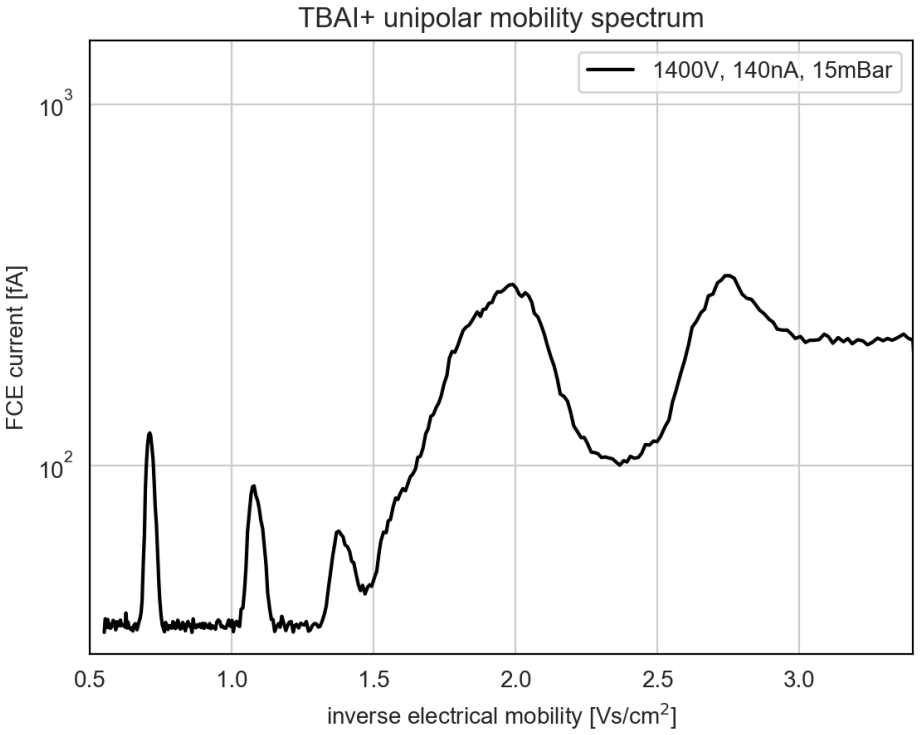

Figure 34: Unipolar mobility spectrum of TBAI+ while operating the UDMA4 at blower setting 8 and the electrospray at 1400V with 15mBar pressure applied.

6.3.2 Bipolar

To demonstrate that this setup can successfully resolve singly charged clusters beyond the unipolar range for TBAI±, this section presents bipolar mobility spectra as well as the full mass spectra for both TBAI+ and TMAI+ obtained by the ioniAPi-ToF. No particle counters were characterized with these substances in the frame of this work, these results are presented in Brilke et al. (2020).

Both the unipolar (grey) and bipolar (black) mobility spectra are presented in Figure 35 for TBAI+. For inverse mobilities larger than 1.5 Vs/cm^2 additional individual mobility peaks appear, this correlates with the results presented for THABr. Moreover, these results demonstrate that the bipolar electrospray source and this setup can be successfully applied for further characterization measurements of clusters of different substances as presented in Brilke et al. (2020).

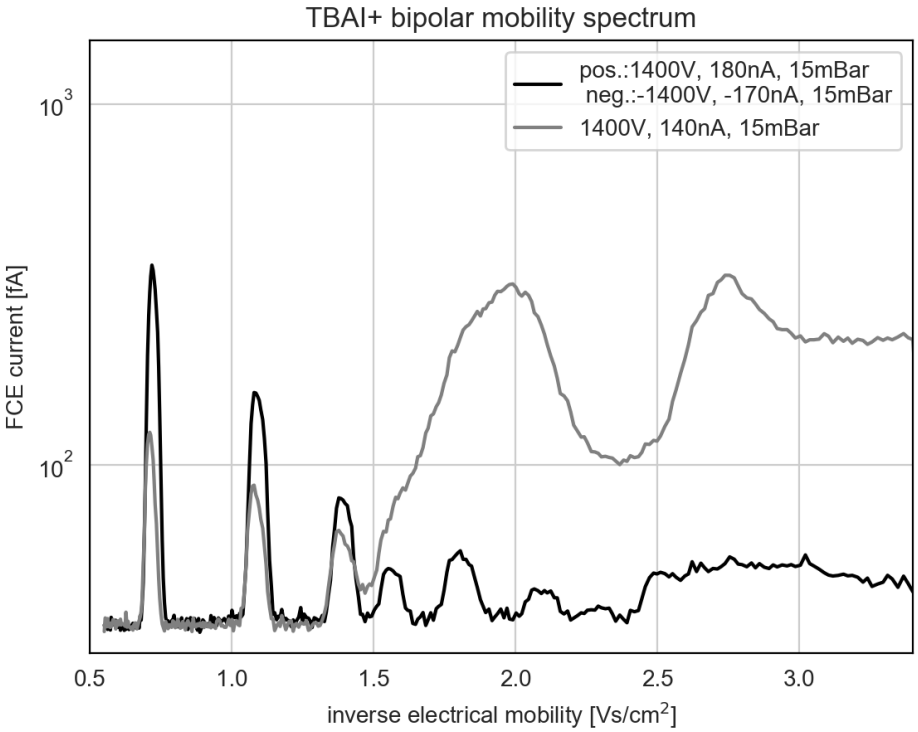

Figure 35: Overlay of the mobility spectra of TBAI+ for unipolar (grey) and bipolar (black) setting of the ES with the UDMA4 blower at setting 8. The complex multiply charged clusters that build the indistinguishable signal for inverse electrical mobilities >1.5 Vs/cm^2 in unipolar mode can be resolved in bipolar mode.

Although the bipolar mobility spectrum for TBAI- shows lower signals compared to the previous spectra recorded, the charge reduction still results in n=5 individually resolvable mobility peaks. Further improvements of the bipolar electrospray settings for this substance might lead to better mobility spectra, as recently demonstrated by Brilke et al. (2020), where successful characterization measurements of different counters were performed with TBAI±. This confirms that the bipolar electrospray source used in combination with this setup can produce singly charged clusters not only for THABr but also for TBAI which can be used to characterize different particle counters.

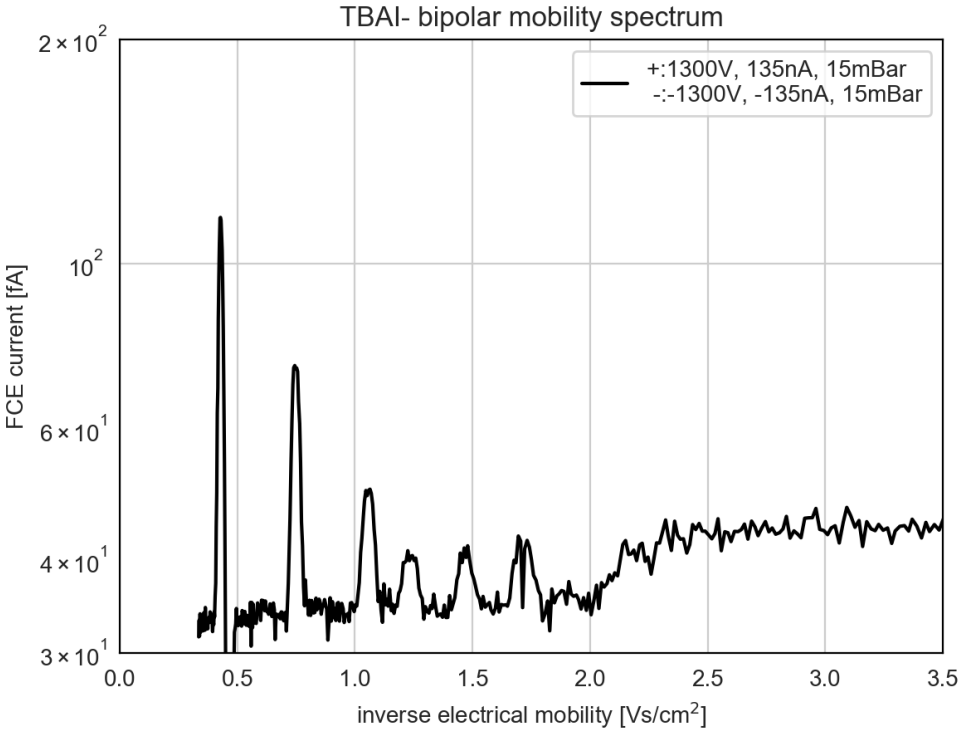

Figure 36: Bipolar mobility spectrum of TBAI- while operating the UDMA4 at blower setting 8 and the electrospray at 1300V for each polarity with 15mBar pressure applied.

The setup given in Figure 17 was used to investigate the masses of the produced TBAI+ signals. A complete mass spectrum of unipolar (blue) and bipolar (red) TBAI+ recorded by the ioniAPi-ToF presenting the first n=8 clusters is given in Figure 37 while averaging over 5 minutes for both modes. Both mass spectra are normalized to the monomer signal. The masses corresponding to TBAI+ clusters are labeled as given in Table 1. The grey markers indicate the approximate masses corresponding to doubly charged clusters. Unlike for the case of THABr [Fernandez de la Mora et al., 2005], the masses of multiply charged clusters of TBAI have not been investigated and can therefore not be labeled specifically. The overall cluster and background signal is higher in unipolar mode, whereas in bipolar mode the significant noise for larger masses between clusters is reduced. For masses smaller than the monomer large signals are detected in both uni- and bipolar mode, these could be associated to cluster fragmentation in the ioniAPi-ToF or the previously mentioned water, acetonitrile or ethanol substances in the system [Heinritzi et al., 2016, Leiminger et al., 2019, Passananti et al., 2019, Brilke et al., 2020].

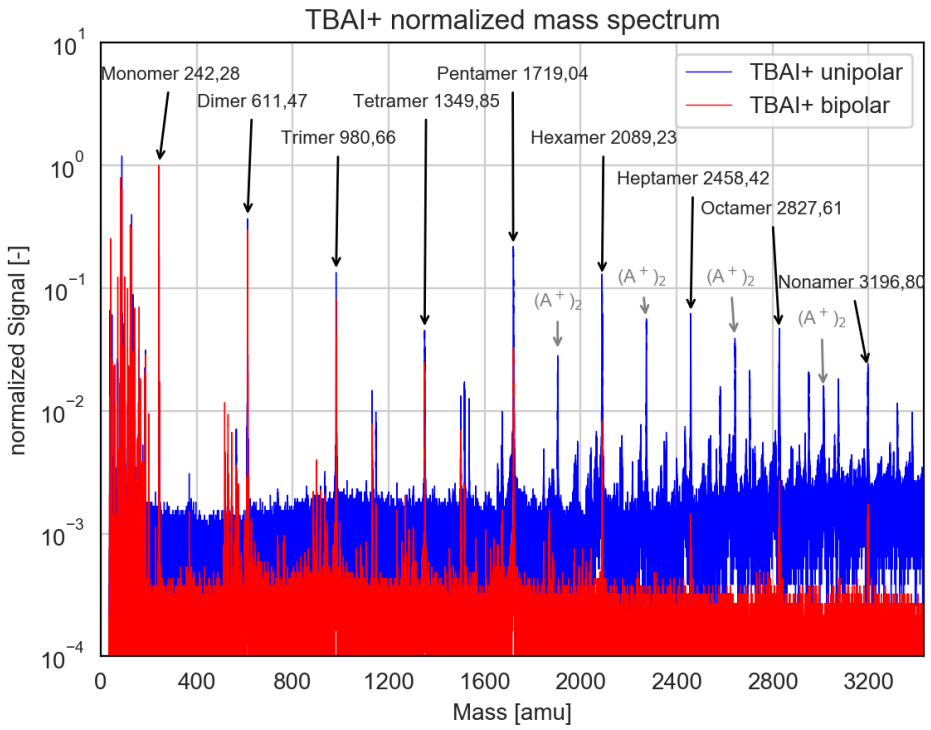

Figure 37: Mass spectrum of spraying TBAI+ in uni-/ and bipolar mode obtained by using the setup given in Figure 17. The spectrum was normalized to the monomer signal. The clusters and their corresponding masses are labeled up to the nonamer (n=8). Similar to the THABr mass spectrum, the doubly charged peaks $(A^+)_2$ are labeled in grey.

To extend the number of possible reference substances which can be used for characterization measurements with the bipolar electrospray source, an averaged mass spectrum over 5 minutes for TMAI+ was recorded to demonstrate that the expected clusters are present in the mass spectra. The different clusters and their corresponding masses are labeled in Figure 38 for both unipolar (blue) and bipolar (red) mode. The spectra are normalized to the monomer and show that significant amounts of uncharacterized ions are detected throughout the mass spectra. For future studies it will be necessary to obtain mobility and mass spectra and investigate the individual mobility peaks to assign their corresponding masses.

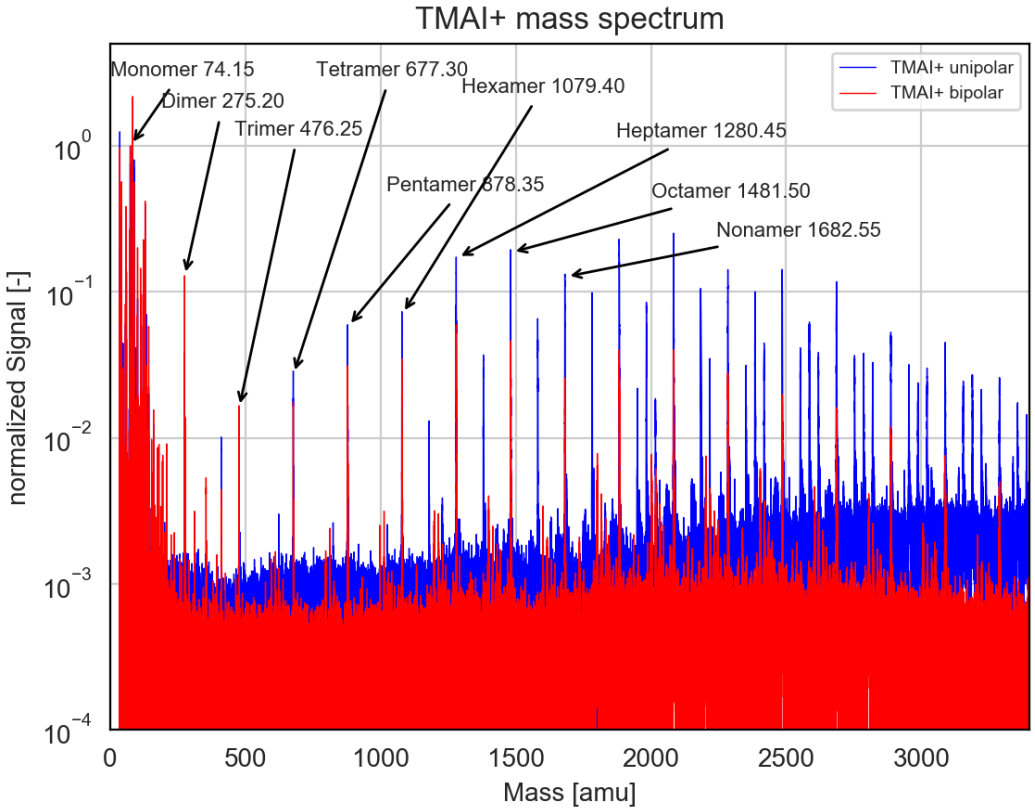

Figure 38: Mass spectrum of spraying TMAI+ in uni-/ and bipolar mode obtained by using the setup given in Figure 17. The spectrum was normalized to the Monomer signal. The clusters and their corresponding masses are labeled up to the nonamer (n=8).

7 Conclusion and Future Outlook

Nanometer sized mobility standards generated by unipolar electrospray ionization have been used to characterize instruments in aerosol research. However this method has been limited to singly charged clusters below 2 nanometers. Beyond this size the salt clusters can not be separated by electrical mobility due to the presence of multiply charged clusters.
In this study a bipolar electrospray source was introduced to reduce the charge states of multiply charged salt clusters. This charge reduction led to dominantly singly charged clusters of THABr and TBAI being produced with this setup. In combination with the UDMA4 mobility standards were generated at high enough concentrations for subsequent analysis and characterization measurements using a newly developed ioniAPi-ToF MS, a fast response FCE and a TSI Model 3776 UCPC. Several mobility spectra for different settings of the bipolar electrospray source were investigated and characterized for further measurements with THABr. The complete mass spectra of THABr, TBAI and TMAI were recorded to confirm the presence of the according singly charged clusters in both unipolar and bipolar mode. Latter showing that the switch to bipolar mode significantly reduces the presence of multiply charged clusters throughout the whole mass range. Optimized settings for voltage, current and pressure enabled subsequent analysis of the mobility peaks to clearly assign higher order clusters to their corresponding masses for THABr+ clusters up to n=6. The stability of the produced signal could be maintained over several hours. After chemical analysis of the mobility spectra with the ioniAPi-ToF MS, the THABr+ mobility standards generated with this system were used to characterize a TSI Model 3776 UCPC. The UCPC was operated at modified temperature settings to increase the supersaturation inside. The previously accessible range of singly charged clusters was successfully extended with this method. The obtained counting efficiency curves not only show that the cut-off diameter aligns with previous investigations, but it furthermore signals the presence of dominantly singly charged clusters. This is highlighted by the efficiency plateau reaching values of 1, whereas the presence of multiply charged clusters would lead to over counting in the FCE and efficiencies lower than 1 would result. These results in combination with the previously obtained mass spectra confirm that indeed dominantly singly charged clusters are present in the classified mobility peaks.
Having confirmed that the bipolar electrospray source in combination with a high resolution DMA is capable of producing mobility standards of precisely known size and composition, qualifies this setup for sub-3nm characterization of CPCs. A possible additional substance beyond THABr and TBAI used for instrument characterization was introduced with TMAI, although future studies will need to characterize the mobility spectra and its behavior in the bipolar electrospray source. Extending the number of used substances will enable a more detailed insight into particle number concentrations and size distribution measurements for the sub-3nm size range used for the investigation of small aerosol particles and new particle formation in the atmosphere.

References

[Attoui et al., 2013] Attoui, M., Paragano, M., Cuevas, J., and Fernandez de la Mora, J. (2013). Tandem DMA Generation of Strictly Monomobile 1–3.5 nm Particle Standards. *Aerosol Science and Technology*, 47(5):499–511.

[Barmpounis et al., 2018] Barmpounis, K., Ranjithkumar, A., Schmidt-Ott, A., Attoui, M., and Biskos, G. (2018). Enhancing the detection efficiency of condensation particle counters for sub-2 nm particles. *Journal of Aerosol Science*, 117(December 2017):44–53.

[Brilke et al., 2020] Brilke, S., Resch, J., Leiminger, M., Steiner, G., Tauber, C., Wlasits, P. J., and Winkler, P. M. (2020). Precision characterization of three ultrafine condensation particle counters using singly charged salt clusters in the 1–4 nm size range generated by a bipolar electrospray source. *Aerosol Science and Technology*, 0(0):1–14.

[Bzdek and Johnston, 2010] Bzdek, B. R. and Johnston, M. V. (2010). New particle formation and growth in the troposphere. *Analytical Chemistry*, 82(19):7871–7878.

[Cheng et al., 1990] Cheng, Y. S., Yamada, Y., Yeh, H. C., and Swift, D. L. (1990). Deposition of ultrafine aerosols in a human oral cast. *Aerosol Science and Technology*, 12(4):1075–1081.

[Colbeck and Lazaridis, 2010] Colbeck, I. and Lazaridis, M. (2010). Aerosols and environmental pollution. *Naturwissenschaften*, 97(2):117–131.

[Cunningham, 1910] Cunningham, E. (1910). On the Velocity of Steady Fall of Spherical Particles through Fluid Medium. *Proceedings of the Royal Society A: Mathematical, Physical and Engineering Sciences*, 83(563):357–365.

[Fenn et al., 1989] Fenn, J., Mann, M., Meng, C., Wong, S., and Whitehouse, C. (1989). Electrospray ionization for mass spectrometry of large biomolecules. *Science*, 246(4926):64–71.

[Fernandez de la Mora, 2018] Fernandez de la Mora, J. (2018). Mobility Analysis of Proteins by Charge Reduction in a Bipolar Electrospray Source. *Analytical Chemistry*, 90(20):12187–12190.

[Fernandez de la Mora and Barrios-Collado, 2017] Fernandez de la Mora, J. and Barrios-Collado, C. (2017). A bipolar electrospray source of singly charged salt clusters of precisely controlled composition. *Aerosol Science and Technology*, 51(6):778–786.

[Fernandez de la Mora et al., 2005] Fernandez de la Mora, J., Thomson, B. A., and Gamero-Castaño, M. (2005). Tandem mobility mass spectrometry study of electrosprayed tetraheptyl ammonium bromide clusters. *Journal of the American Society for Mass Spectrometry*, 16(5):717–732.

[Flagan, 1998] Flagan, R. C. (1998). History of Electrical Aerosol Measurements. *Aerosol Science and Technology*, 28(4):301–380.

[Flagan, 1999] Flagan, R. C. (1999). On Differential Mobility Analyzer Resolution. *Aerosol Science and Technology*, 30(6):556–570.

[Gordon et al., 2017] Gordon, H., Kirkby, J., Baltensperger, U., Bianchi, F., Breitenlechner, M., Curtius, J., Dias, A., Dommen, J., Donahue, N. M., Dunne, E. M., Duplissy, J., Ehrhart, S., Flagan, R. C., Frege, C., Fuchs, C., Hansel, A., Hoyle, C. R., Kulmala, M., Kürten, A., Lehtipalo, K., Makhmutov, V., Molteni, U., Rissanen, M. P., Stozkhov, Y., Tröstl, J., Tsagkogeorgas, G., Wagner, R., Williamson, C., Wimmer, D., Winkler, P. M., Yan, C., and Carslaw, K. S. (2017). Causes and importance of new particle formation in the present-day and preindustrial atmospheres. *Journal of Geophysical Research: Atmospheres*, 122(16):8739–8760.

[Heinritzi et al., 2016] Heinritzi, M., Simon, M., Steiner, G., Wagner, A. C., Kürten, A., Hansel, A., and Curtius, J. (2016). Characterization of the mass-dependent transmission efficiency of a CIMS. *Atmospheric Measurement Techniques*, 9(4):1449–1460.

[Hinds, 1999] Hinds, W. C. (1999). *Aerosol Technology: Properties, Behavior, and Measurement of Airborne Particles*. John Wiley & Sons, Inc., 2nd edition.

[Intra and Tippayawong, 2009] Intra, P. and Tippayawong, N. (2009). Measurements of ion current from a corona-needle using a faraday cup electrometer. *Chiang Mai Journal of Science*, 36(1):110–119.

[Intra and Tippayawong, 2015] Intra, P. and Tippayawong, N. (2015). Development and Evaluation of a Faraday Cup Electrometer for Measuring and Sampling Atmospheric Ions and Charged Aerosols. *Particulate Science and Technology*, 33(3):257–263.

[IPCC, 2013] IPCC (2013). Clouds and aerosols. *Climate Change 2013 the Physical Science Basis: Working Group I Contribution to the Fifth Assessment Report of the Intergovernmental Panel on Climate Change*, 9781107057:571–658.

[Jiang et al., 2011] Jiang, J., Chen, M., Kuang, C., Attoui, M., and McMurry, P. H. (2011). Electrical mobility spectrometer using a diethylene glycol condensation particle counter for measurement of aerosol size distributions down to 1 nm. *Aerosol Science and Technology*, 45(4):510–521.

[Junninen et al., 2010] Junninen, H., Ehn, M., Petäjä, Luosujärvi, L., Kotiaho, T., Kostiainen, R., Rohner, U., Gonin, M., Fuhrer, K., Kulmala, M., and Worsnop, D. R. (2010). A high-resolution mass spectrometer to measure atmospheric ion composition. *Atmospheric Measurement Techniques*, 3(4):1039–1053.

[Kangasluoma, 2015] Kangasluoma, J. (2015). *Generation , characterization and sizing of sub-3 nm nanoparticles and molecular clusters*. Phd thesis, University of Helsinki.

[Kangasluoma et al., 2013] Kangasluoma, J., Junninen, H., Lehtipalo, K., Mikkilä, J., Vanhanen, J., Attoui, M., Sipilä, M., Worsnop, D., Kulmala, M., and Petäjä, T. (2013). Remarks on Ion Generation for CPC Detection Efficiency Studies in Sub-3-nm Size Range. *Aerosol Science and Technology*, 47(5):556–563.

[Kangasluoma et al., 2014] Kangasluoma, J., Kuang, C., Wimmer, D., Rissanen, M. P., Lehtipalo, K., Ehn, M., Worsnop, D. R., Wang, J., Kulmala, M., and Petäjä, T. (2014). Sub-3 nm particle size and composition dependent response of a nano-CPC battery. *Atmospheric Measurement Techniques*, 7(3):689–700.

[Knutson and Whitby, 1975] Knutson, E. and Whitby, K. (1975). Aerosol classification by electric mobility: apparatus, theory, and applications. *Journal of Aerosol Science*, 6(6):443–451.

[Kulmala et al., 2013] Kulmala, M., Kontkanen, J., Junninen, H., Lehtipalo, K., Manninen, H. E., Nieminen, T., Petaja, T., Sipila, M., Schobesberger, S., Rantala, P., Franchin, A., Jokinen, T., Jarvinen, E., Aijala, M., Kangasluoma, J., Hakala, J., Aalto, P. P., Paasonen, P., Mikkila, J., Vanhanen, J., Aalto, J., Hakola, H., Makkonen, U., Ruuskanen, T., Mauldin, R. L., Duplissy, J., Vehkamaki, H., Back, J., Kortelainen, A., Riipinen, I., Kurten, T., Johnston, M. V., Smith, J. N., Ehn, M., Mentel, T. F., Lehtinen, K. E. J., Laaksonen, A., Kerminen, V.-M., and Worsnop, D. R. (2013). Direct Observations of Atmospheric Aerosol Nucleation. *Science*, 339(6122):943–946.

[Leiminger et al., 2019] Leiminger, M., Feil, S., Mutschlechner, P., Ylisirniö, A., Gunsch, D., Fischer, L., Jordan, A., Schobesberger, S., Hansel, A., and Steiner, G. (2019). Characterisation of the transfer of cluster ions through an atmospheric pressure interface time-of-flight mass spectrometer with hexapole ion guides. *Atmospheric Measurement Techniques*, 12(10):5231–5246.

[Mäkelä et al., 1996] Mäkelä, J. M., Riihelä, M., Ukkonen, A., Jokinen, V., and Keskinen, J. (1996). Comparison of mobility equivalent diameter with Kelvin-Thomson diameter using ion mobility data. *The Journal of Chemical Physics*, 105(4):1562–1571.

[McMurry, 2000] McMurry, P. H. (2000). The History of Condensation Nucleus Counters. *Aerosol Science and Technology*, 33(4):297–322.

[Mönkkönen et al., 2004] Mönkkönen, P., Koponen, I. K., Lehtinen, K. E. J., Hämeri, K., Uma, R., and Kulmala, M. (2004). Measurements in a highly polluted Asian mega city: observations of aerosol number size distribution, modal parameters and nucleation events. *Atmospheric Chemistry and Physics Discussions*, 4(5):5407–5431.

[Passananti et al., 2019] Passananti, M., Zapadinsky, E., Zanca, T., Kangasluoma, J., Myllys, N., Rissanen, M. P., Kurtén, T., Ehn, M., Attoui, M., and Vehkamäki, H. (2019). How well can we predict cluster fragmentation inside a mass spectrometer? *Chemical Communications*, 55(42):5946–5949.

[Reischl, 1991] Reischl, G. P. (1991). Measurement of Ambient Aerosols by the Differential Mobility Analyzer Method: Concepts and Realization Criteria for the Size Range Between 2 and 500 nm. *Aerosol Science and Technology*, 14(1):5–24.

[Spracklen et al., 2008] Spracklen, D. V., Carslaw, K. S., Kulmala, M., Kerminen, V. M., Sihto, S. L., Riipinen, I., Merikanto, J., Mann, G. W., Chipperfield, M. P., Wiedensohler, A., Birmili, W., and Lihavainen, H. (2008). Contribution of particle formation to global cloud condensation nuclei concentrations. *Geophysical Research Letters*, 35(6):1–5.

[Steiner, 2011] Steiner, G. (2011). *High Resolution Mobility Spectrometry Of Molecular Ions And Their Effect On The Charging Probabilities Of Airborne Particles Under Bipolar Diffusion Charging Conditions*. Phd thesis, University of Vienna.

[Steiner et al., 2010] Steiner, G., Attoui, M., Wimmer, D., and Reischl, G. P. (2010). A medium flow, high-resolution Vienna DMA running in recirculating mode. *Aerosol Science and Technology*, 44(4):308–315.

[Steiner et al., 2017] Steiner, G., Franchin, A., Kangasluoma, J., Kerminen, V.-M., Kulmala, M., and Petäjä, T. (2017). Production of neutral molecular clusters by controlled neutralization of mobility standards. *Aerosol Science and Technology*, 51(8):946–955.

[Steiner et al., 2018] Steiner, G., Orzan, M., Nagler, I., Petrakakis, E., Selimovic, M., Tauber, C., and Tettich, F. (2018). Improving airborne nanoparticle and cluster detection with the butanol based laminar flow condensation nuclei counters Grimm 5 . 403 and 5 . 412 . pages 2–3.

[Stolzenburg and McMurry, 1991] Stolzenburg, M. R. and McMurry, P. H. (1991). An ultrafine aerosol condensation nucleus counter. *Aerosol Science and Technology*, 14(1):48–65.

[Takegawa et al., 2017] Takegawa, N., Iida, K., and Sakurai, H. (2017). Modification and laboratory evaluation of a TSI ultrafine condensation particle counter (Model 3776) for airborne measurements. *Aerosol Science and Technology*, 51(2):235–245.

[Tauber et al., 2019a] Tauber, C., Brilke, S., Wlasits, P. J., Bauer, P. S., Köberl, G., Steiner, G., and Winkler, P. M. (2019a). Humidity effects on the detection of soluble and insoluble nanoparticles in butanol operated condensation particle counters. *Atmospheric Measurement Techniques*, 12(7):3659–3671.

[Tauber et al., 2019b] Tauber, C., Steiner, G., and Winkler, P. M. (2019b). Counting efficiency determination from quantitative intercomparison between expansion and laminar flow type condensation particle counter. *Aerosol Science and Technology*, 53(3):344–354.

[Taylor, 1964] Taylor, G. (1964). Disintegration of water drops in an electric field. *Proceedings of the Royal Society of London. Series A. Mathematical and Physical Sciences*, 280(1382):383–397.

[TSI, 2019] TSI (2019). TSI Model 3776 Ultrafine Condensation Particle Counter - Operation and Service Manual, https://www.wmo-gaw-wcc-aerosol-physics.org/files/cpc-3776.pdf.

[Ude, 2004] Ude, S. (2004). *Measurement and properties of nanometer particles in the gas phase*. Phd thesis, Yale University.

[Ude and Fernández de la Mora, 2005] Ude, S. and Fernández de la Mora, J. (2005). Molecular monodisperse mobility and mass standards from electrosprays of tetra-alkyl ammonium halides. *Journal of Aerosol Science*, 36(10):1224–1237.

[Wimmer et al., 2013] Wimmer, D., Lehtipalo, K., Franchin, A., Kangasluoma, J., Kreissl, F., Kürten, A., Kupc, A., Metzger, A., Mikkilä, J., Petäjä, T., Riccobono, F., Vanhanen, J., Kulmala, M., and Curtius, J. (2013). Performance of diethylene glycol-based particle counters in the sub-3 nm size range. *Atmospheric Measurement Techniques*, 6(7):1793–1804.

[Winklmayr et al., 1991] Winklmayr, W., Reischl, G., Lindner, A., and Berner, A. (1991). A new electromobility spectrometer for the measurement of aerosol size distributions in the size range from 1 to 1000 nm. *Journal of Aerosol Science*, 22(3):289–296.